ASM Handbook, Volume 9: Metallography and Microstructures
G.F. Vander Voort, editor, p428–447
DOI: 10.1361/asmhba0003759

Quantitative Characterization and Representation of Global Microstructural Geometry

Arun M. Gokhale, Georgia Institute of Technology

IT IS THE CENTRAL PRECEPT of materials science that processing governs microstructure and the microstructure influences the properties and performance of materials. Consequently, quantitative characterization and mathematical representation of microstructure are of considerable importance in materials science. The discipline of quantitative characterization of microstructural geometry is called quantitative metallography or stereology. The objective of quantitative metallography/stereology is to describe the geometric characteristics of the features (for example, grains, voids, precipitates, dislocations) present in the microstructure in quantitative terms, such as amounts (how much?), numbers (how many?), and sizes (how large?).

Material microstructures are three-dimensional and, therefore, the attributes of three-dimensional microstructural geometry are of core interest. Nonetheless, as most of the materials are opaque, the microstructural observations are usually on the two-dimensional (2-D) metallographic sections through the three-dimensional (3-D) microstructural domains of interest. The microstructure observed in a metallographic section consists of intersections of the features in the 3-D microstructure with the sectioning plane. Therefore, in a metallographic plane, the volumes (e.g., grains, voids, particles) in a 3-D microstructure appear as areas, and the surfaces (e.g., grain boundaries, precipitate interfaces) appear as lines. Clearly, a 2-D metallographic section does not contain all the information concerning the true 3-D microstructural geometry. Even so, numerous important geometric attributes of 3-D microstructures can be estimated from the measurements that can be performed on 2-D metallographic sections.

It is well known that material microstructures are of stochastic nature. Consequently, no two microstructures are exactly alike; no two fields of view in a microstructure are exactly alike; and in most microstructures, no two particles/grains in a field of view are exactly alike. It follows that microstructure characterization must be couched in statistical terms. Further, microstructural features have complex morphologies, their locations and orientations are often nonuniform, and spatial clustering and correlations frequently exist. Accordingly, quantitative metallographic techniques must be free of any restrictive geometric assumptions so that they can be successfully applied to any arbitrary microstructure. Despite these complexities, quantitative metallographic procedures are straightforward to use in practice. Numerous geometric attributes of three-dimensional microstructures can be estimated in an unbiased manner from the counting measurements that can be performed on representative metallographic planes, without involving any assumptions whatsoever.

Modern quantitative metallographic/stereological methods typically involve statistical sampling of 3-D microstructure using lower dimensional geometric test probes such as planes, lines, and points. In many cases, the basic measurements simply consist of counting the number of times the test probe intersects (or hits) the microstructural features of interest; the average value (or more precisely, statistical expected value) of such "hits" is uniquely related to specific geometric attributes of the 3-D microstructure through simple stereological equations. The stereological techniques have rigorous theoretical foundations that are anchored in the disciplines of stochastic geometry (Ref 1), integral geometry and global analysis (Ref 2), and differential geometry (Ref 3). The stereological methods are completely general, and therefore they are also applicable to microstructures encountered in many other disciplines, including biology (Ref 4) and mineralogy (Ref 5).

The basic principles of classical quantitative metallography are covered in numerous books (Ref 6–8). Nevertheless, during the past decade or so, there has been substantial progress in the development of new design-based stereological techniques for efficient characterization of anisotropic microstructures (Ref 9–18) and new techniques for unbiased estimation of number density of microstructural features (Ref 19–21). Further, advances in digital image processing techniques (Ref 22–28), new microscopy techniques (Ref 29–31), and availability of powerful digital image analysis systems have opened up a whole new era of quantitative metallography dealing with new efficient techniques for reconstruction of 3-D microstructure from serial sections (Ref 32–35) and new techniques for characterization parameters such as microstructural spatial correlations and clustering (Ref 12, 22, 23, 35–37), coordination number distributions (Ref 35), and bivariate and trivariate size-shape-orientation distributions of particles/inclusions in 3-D microstructures (Ref 38, 39). There has also been a steady rise in the practical applications of quantitative metallography during the recent years (Ref 40–60).

The geometric attributes of microstructural features can be divided into the following categories:

- Numerical extents of microstructural features (how much?)
- Number density of microstructural features (how many?)
- Derived microstructural properties (grain size, mean free path, etc.)
- Feature specific size, shape, and orientation distributions
- Descriptors of microstructural spatial clustering and correlations

The classical methods as well as new design-based quantitative metallographic techniques for the estimation of the above categories of microstructural attributes are presented in this article; the emphasis is on the practical aspects of the measurement techniques and applications. The next section of this article describes the quantitative metallographic procedures for estimation of the numerical extents (amounts) of the fea-

tures in microstructure, and that is followed by the techniques for estimation of number density, derived properties, and particle size distributions.

Numerical Extents of Microstructural Features (How Much?)

Numerical extent specifies total "amount" of microstructural features of interest per unit volume of microstructure. Volume fraction (or volume percentage) is the numerical extent of the amount of a phase (or constituent) in a unit volume of 3-D microstructure. On the other hand, total surface area per unit volume characterizes the numerical extent of two-dimensional internal surfaces/interfaces. Similarly, total length per unit microstructural volume (or so-called length density) represents the amount of one-dimensional lineal features of interest in a 3-D microstructure. These first-order microstructural parameters are of central importance in materials science as they influence numerous material properties. The classical quantitative metallographic techniques permit efficient estimation of volume fraction, total surface area per unit volume, and total length of lineal features of interest per unit volume in any isotropic uniform random 3-D microstructure from the counting measurements that can be performed in 2-D metallographic sections/projected images (Ref 6–8, 61). Such measurements have been used in numerous experimental studies on processing-microstructure-properties relationships (Ref 27, 40–42, 44, 46, 48, 51–54). Recent developments in design-based stereology enable efficient estimation of total surface area per unit volume and total length per unit volume in the anisotropic microstructures as well (Ref 9–18). These design-based stereological measurements have also been used in several recent experimental studies (Ref 11, 43, 45, 55–58, 62–69). The quantitative metallographic methods for estimation of volume fraction, total surface area per unit volume, and the total length of per unit volume are described in the following sections.

Volume Fraction

Volume fraction is an important measure of the relative amount of a phase in a microstructure. It is equal to the sum of the volumes of the regions of a phase of interest in a material specimen divided by the volume of the specimen. Therefore, the volume fraction of a phase is the fraction of the 3-D microstructural space occupied by that phase. Volume fraction is denoted by the symbol, V_V where the subscript V signifies the normalization by the specimen volume. Obviously, the volume fraction of a phase must always be in the range $0 \leq V_V \leq 1$. Further, the sum of the volume fractions of all the phases in a microstructure must be equal to one. Volume fraction is often represented in terms of volume percentage, which is simply equal to volume fraction multiplied by 100.

The volume fraction of a phase in a microstructure is governed by the chemistry and processing history of the material. Numerous material properties depend on volume fractions of different phases in microstructure (Ref 40, 42, 46, 47–49, 52, 55). For example, the tendency of delayed cracking of quenched steel depends on the relative amount of retained austenite, the volume fraction of porosity in alumina controls its optical properties, and the strength of a fiber composite depends on the relative amounts of the fibers and the matrix. Accordingly, volume fraction is the most frequently measured microstructural attribute.

Volume fraction of a phase in any arbitrary 3-D microstructure can be estimated from the measurements performed in the 2-D metallographic sections without involving any assumptions concerning the shapes, sizes, orientations, or spatial randomness of the features of interest. Interestingly, as volume fraction is a dimensionless microstructural parameter, it is not necessary to know the microscope (or micrograph) magnification for its estimation. Volume fraction can be estimated from the measurements performed in the metallographic planes either by using the areal analysis method, or by using the point counting method. These techniques are described in the following paragraphs.

Areal Analysis. In 1848, French geologist Delesse developed the areal analysis technique for estimation of volume fraction (Ref 6). The areal analysis involves the measurement of the fraction of the area of representative metallographic planes A_A occupied by the phase of interest. The population average value (or more precisely, "expected value") $\langle A_A \rangle$ of the area fraction A_A is equal to the volume fraction V_V of that phase in the 3-D microstructure (Ref 4–8):

$$V_V = \langle A_A \rangle \quad \text{(Eq 1)}$$

The area fraction of the phase of interest A_A can be measured in the microstructural fields observed in a microscope, or from micrographs. Obviously, there are statistical variations in the local area fraction A_A measured in different microstructural fields. Therefore, it is essential to perform the measurements on numerous microstructural fields to obtain a representative average value of the area fraction. Areal analysis is a convenient method for estimation of volume fraction using digital image analysis. Once a gray-scale microstructural image (Fig. 1a) is converted into its binary image (Fig. 1b), the local area fraction of the phase of interest is simply equal to the number of pixels in the phase of interest divided by the total number of pixels in the measurement frame. Modern image analyzers can be interfaced with automatic specimen movement stage and autofocus modules of the microscope to automatically scan large number (~100 or more) of microstructural fields at certain fixed distance intervals and perform area fraction measurements in such microstructural fields automatically to yield a precise average value of the volume fraction. Nonetheless, in some microstructures, it is difficult to obtain a representative binary image from gray scale microstructural image (for example, microstructure in Fig. 2a). In such cases, digital image analysis is not useful, and one must resort to manual measurements. Areal analysis is not an efficient technique for estimation of volume fraction if manual measurements are required. In such cases, volume fraction can be efficiently estimated by using the point counting method discussed next.

Point Counting. In this method, a set of test points is overlaid on a microstructural field, and the number of test points contained in the phase of interest is counted. The fraction of test points in the phase of interest P_P is calculated by dividing the number of test points in phase of interest by the total number of test points. The population average value of this point fraction $\langle P_P \rangle$ is precisely equal to the volume fraction of the phase of interest (Ref 4–8):

$$V_V = \langle P_P \rangle \quad \text{(Eq 2)}$$

The point counting can be performed by using a grid of regular array of test points, or by using

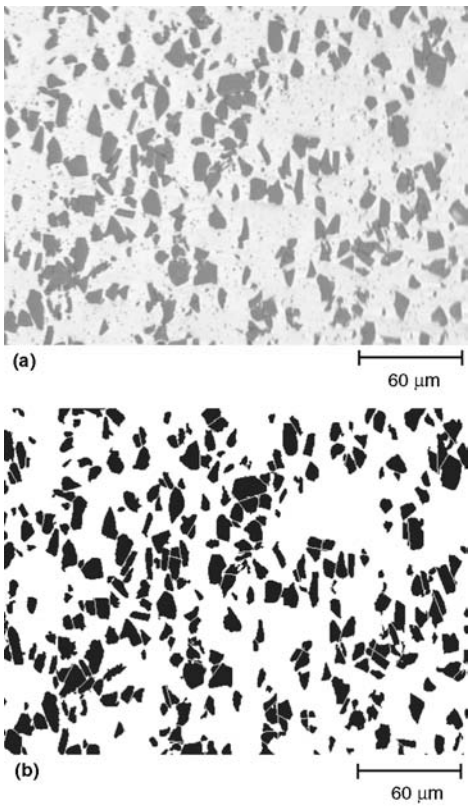

Fig. 1 Areal analysis. (a) Gray scale microstructural image of a metal-matrix composite depicting SiC particles in an aluminum alloy matrix. (b) Binary image of microstructure in (a) depicting excellent segmentation of the SiC particles as the dark phase. The area fraction of SiC particles in this image is equal to the number of black pixels divided by the total number of pixels in the image.

randomly distributed test points. The procedure is called "systematic" point counting, when a regular array of points is used, and it is called "random" point counting when random test points are used. The systematic point counting is easier to perform in practice, and it is more efficient than the random point counting. Figure 2(b) illustrates the systematic point counting procedure using an array of test points. The efficiency of systematic point counting can be further increased by placing the test point grid at regular intervals in the metallographic plane rather than at independent random locations, and sampling multiple planes (if necessary) at different locations at fixed distance intervals in the specimen of interest. Figure 3 illustrates such a multilevel systematic sampling scheme, where all the regions of the specimen get equal "weightage." Such systematic sampling procedure is superior to the independent random sampling for all the quantitative microstructural measurements (Ref 6, 7, 16, 70–74). Volume fraction measurements are extremely useful for characterizing the effects of process parameters on microstructure as well as to correlate the effects of relative amounts of different phases on the properties and performance of materials. For example, Figure 4 illustrates the effect of hot-rolling temperature on the volume fraction of recrystallized regions in a set of specimens of 7050 wrought aluminum alloy, where the recrystallized volume fraction was measured manually using the systematic point counting method (Ref 55).

Several stereologists have carried out rigorous statistical analyses of the bias, efficiency, and precision of different measurement procedures for volume fraction estimation. Their conclusions are (Ref 6, 7, 70–72):

- Both the areal analysis and point counting are statistically unbiased and general methods. These techniques do not involve any assumptions concerning sizes and/or shapes of the features of the phase of interest.
- The angular orientations of the regions of the phase of interest need not be random; the techniques are equally applicable to anisotropic microstructures.
- It is not necessary to randomize the angular orientation of the sectioning plane, even for anisotropic microstructures. The measurements can be performed in a set of parallel planes of any one convenient angular orientation at systematic random locations in the 3-D microstructure.
- The regions of the phase of interest need not be randomly located in the sample; they may be at any arbitrary location, as long as the sampling is systematic random (or independent random) with respect to the phase of interest. Further, as this locational randomness of the sectioning plane is required only with respect to the phase of interest, if the regions of the phase of interest are randomly located in the microstructure, then measurements in a single sectioning plane (not necessarily randomly located or oriented) can yield a reliable estimate of V_V.
- If the microstructure contains a gradient, then it is more efficient to perform the measurements on the metallographic planes that contain the gradient.
- For optimal efficiency and precision, the measurements should be performed at the lowest magnification where all the features of interest are clearly resolved. Any further increase in the magnification decreases the efficiency.
- For manual measurements, systematic point counting (Fig. 2 and 3) is the most efficient sampling procedure.

Estimation of volume fraction involves statistical sampling of microstructure, and consequently there is always a statistical sampling error associated with the estimated value of the volume fraction. Nevertheless, the sampling error can be kept as small as desired simply by performing the measurements on more microstructural fields in more metallographic planes. The nature of the statistical sampling error and its estimation are described in the next paragraph.

Estimation of Sampling Error. Consider the estimation of volume fraction using a grid of test points containing P_T number of points. Suppose this grid is placed at n different locations in the microstructure, and each time, the number of test points in the phase of interest is counted. Let P_1, P_2, . . ., P_i, . . . P_n represent these data, which essentially constitute a statistical sample of size n. The estimated value of the population average point fraction $\langle P_P \rangle$ with the associated confidence interval is given as:

$$\langle P_P \rangle = [\Sigma P_i/(n \cdot P_T)] \pm E_n \qquad \text{(Eq 3)}$$

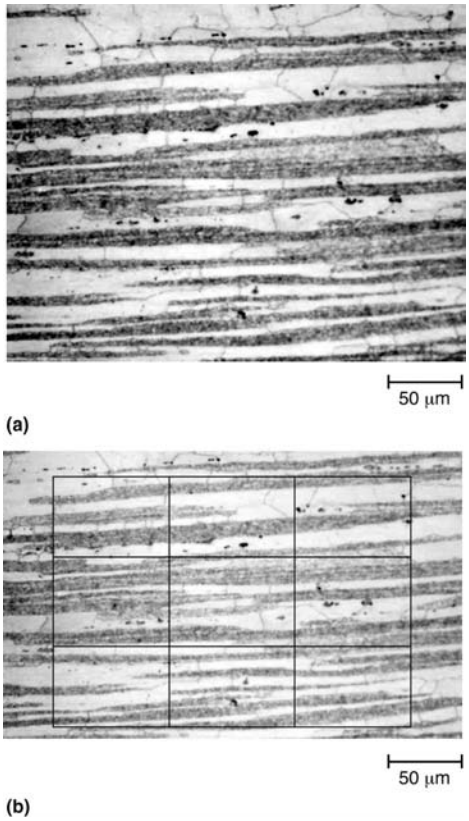

Fig. 2 Microstructure that is not suitable for areal analysis techniques. (a) Microstructure of a hot-rolled partially recrystallized 7050 aluminum alloy containing large anisotropic recrystallized grains and unrecrystallized regions containing subgrains. In such microstructures digital image analysis is not useful for estimation of volume fraction of recrystallized regions as such regions cannot be accurately segmented by the image analyzer. (b) A systematic grid of 16 test points overlaid on the microstructure in (a) to estimate volume fraction of recrystallized regions manually using point counting. Out of total of 16 test points, 7 are contained in the large bright anisotropic recrystallized regions. Therefore, the local point fraction P_P for the recrystallized regions is equal to $^7/_{16}$.

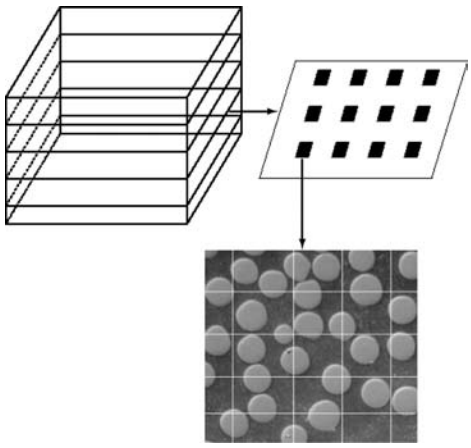

Fig. 3 Multilevel systematic sampling. The first metallographic plane is chosen at a random location in the specimen, and the subsequent planes are sampled such that the planes uniformly cover the specimen and the distance between the planes is approximately the same. Next, in each metallographic plane, the first field is chosen at a random location, and the subsequent fields are systematically chosen such that the distance between consecutive fields is approximately the same and the set of fields uniformly cover the plane. Finally, in each field of view a systematic test probe is placed. For point counting, the probe consists of grid of test points, and the test points contained in the phase of interest are counted.

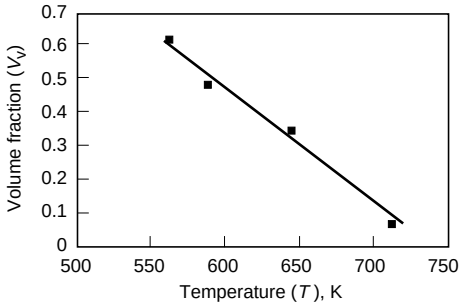

Fig. 4 Experimentally observed quantitative correlation between the volume fraction of recrystallized regions and hot-rolling temperature in a wrought 7050 aluminum alloy (Ref 55)

where E_n is the sampling error. If the sample size n is sufficiently large (for most microstructures, $n > 50$) then E_n can be computed by using (Ref 6, 7):

$$E_n = 2\{\Sigma(\langle P_P\rangle - P_i)^2/[n(n-1)(P_T)^2]\}^{1/2} \quad \text{(Eq 4)}$$

where $\langle P_P\rangle$ is equal to $[\Sigma P_i/n]$, which is the average number of test points in the phase of interest in the sample consisting of n placements of the grid having P_T test points. Combining Eq 2 to 4 gives the following working equation for calculation of the confidence interval in volume fraction estimated from the experimental point counting data:

$$V_V = \langle P_P\rangle = \left[\Sigma P_i/(n\cdot P_T)\right] \pm 2\left\{\Sigma\left(\langle P_P\rangle - P_i\right)^2/\left[n(n-1)(P_T)^2\right]\right\}^{1/2} \quad \text{(Eq 5)}$$

Equation 5 states that there is 95% probability that the true volume fraction of the phase of interest is within the interval given by this equation. Note that the sampling error E_n strongly depends on the sample size n, and therefore it can be kept as small as desired by increasing the sample size n, that is, the number of grid placements. If the sample size is not sufficiently large (i.e., $n < 50$), then other statistical procedures must be used to compute the confidence interval, which are explained elsewhere (Ref 75).

Total Surface Area Per Unit Volume. Microstructures often contain internal surfaces or boundaries such as grain boundaries, precipitate-matrix interfaces, surfaces of internal voids/cavities, and so forth. The total area of the internal microstructural surfaces of interest per unit volume of microstructure is the ratio of the sum of the areas of all the internal surfaces of interest contained in a specimen divided by the volume of the specimen, and it is denoted by the symbol S_V, where the subscript V signifies the normalization by the specimen volume. Figure 5 illustrates this definition of total surface area per unit volume. In two microstructures having the same volume fraction of a phase, S_V is higher in the microstructure having a finer dispersion of that phase. Therefore, S_V can be used to characterize how fine (or coarse) a microstructure is. The mechanical and physical properties of materials strongly depend on the geometric characteristics of the microstructural internal surfaces such as the total area of the grain boundaries. For example, yield stress of a polycrystalline metal increases with the increase in the total surface area of the grain boundaries per unit volume, S_V. This is also a useful parameter for monitoring evolution of microstructure during the processes such as particle coarsening and grain growth, where the driving force is reduction in the total area of the microstructural interfaces. The dimensions of S_V are $\mu m^2/\mu m^3$ or $(\mu m)^{-1}$. Since S_V is not a dimensionless parameter, it is essential to know the magnification of microscope (or micrographs) for its estimation.

Estimation of S_V involves statistical sampling of the 3-D microstructure by test lines. The number of intersections between the test lines and the surfaces of interest is counted. The population average value of the number of intersections between the test lines and the surfaces of interest per unit test line length $\langle I_L\rangle$ is related to the total surface area per unit volume S_V through the stereological equation given by Smith and Guttman (Ref 61) and Saltykov (Ref 8):

$$S_V = 2\langle I_L\rangle \quad \text{(Eq 6)}$$

Equation 6 is general: it is applicable to microstructural surfaces of any arbitrary geometry. I_L has units of $(\mu m)^{-1}$ because it is the number of intersections per unit test line length. In practice, the test lines are placed in a metallographic plane to perform the intersection counting.

An alternate general and unbiased stereological relationship is available for estimation of S_V, which is particularly attractive when the measurements are performed using automatic digital image analysis. This method requires measurements of the total length of all the boundary traces observed per unit area of metallographic plane, L_A. It can be shown that (Ref 61):

$$S_V = [4/\pi]\langle L_A\rangle \quad \text{(Eq 7)}$$

where $\langle L_A\rangle$ is the population average value of the total boundary length per unit area.

It is easier to program an image analyzer to measure the lengths of all the boundaries of interest in the measurement frame as compared to counting the number of intersections of test lines with the boundaries of interest. Some commercial image analyzers are not even equipped with the computer codes for automatic line intersection counting (i.e., I_L measurements). Therefore, if automatic image analysis is to be used, Eq 7 is useful for estimation of S_V. Although, in principle, Eq 6 and 7 are applicable to isotropic as well as anisotropic microstructures, to maximize the efficiency and precision of the estimation procedure somewhat different sampling strategies are needed for practical applications of these stereological equations to isotropic and anisotropic microstructures.

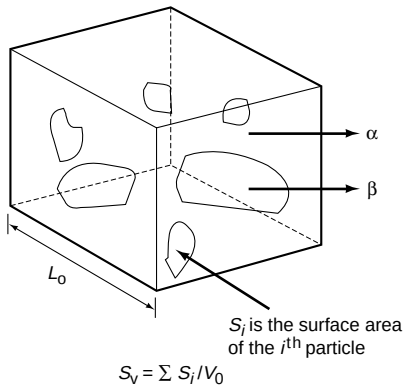

Fig. 5 Definition of S_V. See text for details.

Estimation of S_V in Isotropic Microstructures. In an isotropic microstructure (for example, Fig. 6), the microstructural surfaces have uniform random angular orientations. Consequently, the number of intersections between the test lines and the boundaries/surfaces of interest does not vary systematically with the angular orientation of the test lines. For example, in Fig. 6, on the average, horizontal, or vertical test lines (or lines having any other orientation) of the same length yield statistically similar number of intersections with the pore surfaces. Therefore, in an isotropic microstructure, it is not necessary to perform the intersection counts with test lines and/or metallographic planes of different angular orientations: the measurements on metallographic plane(s) of any one convenient angular orientation using test lines of any one convenient angular orientation can yield a reliable estimate of the population average value of the intersection count $\langle I_L\rangle$. An example of I_L measurements in the isotropic microstructure of sintered NiAl and aluminum mixture containing porosity is given in Fig. 6. In such homogeneous isotropic microstructures, the measurements on about 50 systematic random microstructural fields in just one metallographic plane can yield a reliable estimate of S_V. Even when the measurements are performed manually, this does not take more than about 40 min. Thus, unbiased and precise stereological estimation of S_V in the isotropic microstructures is straightforward and efficient.

Estimation of S_V in Anisotropic Microstructures. In an anisotropic microstructure, the microstructural surfaces have preferred orientations. As a result, the intersection count I_L systematically varies with the angular orientation of the test lines. Figure 7 shows an anisotropic microstructure depicting grain boundaries in a cold-rolled extra-low-carbon steel specimen. Clearly, in such a microstructure, on the average, a horizontal test line is expected to intersect significantly fewer grain boundaries as compared to a

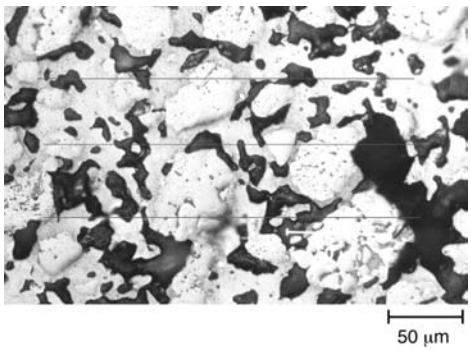

Fig. 6 Intersection counting is illustrated using a set of three horizontal test lines overlaid on the microstructure of a sintered material containing NiAl, aluminum, and porosity. In this microstructure, the pores (dark regions) have no preferred orientations, and the pore surfaces are randomly oriented. The total number of intersections between the pore surfaces and three horizontal test lines is equal to 10 + 13 +17 = 40. The effective length of each test line is 190 μm. Therefore, $I_L = 40/(3 \times 190) = 0.070$ per μm.

vertical test line of the same length. If I_L varies systematically with angular orientation of the test lines, it is essential to perform the intersection counts using test lines of several random angular orientations placed in numerous metallographic planes having random angular orientations to obtain an unbiased and precise estimate of the population average value $\langle I_L \rangle$, which makes the procedure very laborious. Further, in such an isotropic uniform random (IUR) sampling process, it is not known a priori on the test lines and test planes of how many different orientations the measurement need to be performed for a reliable estimate of S_V, because the answer depends on the morphological orientation distribution function of the surfaces of interest (which is usually unknown). During the recent years, a practical and efficient solution to this complex problem has been developed using design-based stereology and vertical section sampling technique (Ref 9) described below.

To begin the sampling process, choose a reference direction in the 3-D space. In the present context, this reference direction is called vertical axis or vertical direction (it has no relation whatsoever to the gravitational vertical). Any plane that contains the vertical axis is called a vertical plane (see Fig. 8 and 9). Baddeley, Gundersen, and Cruz Orive (Ref 9) have shown that the set of vertical planes belonging to any chosen vertical axis contains test lines of all possible angular orientations in the 3-D space. Therefore, for estimation of S_V, it is sufficient to perform the intersection counts using the test lines in any one set of vertical metallographic planes (i.e., there is no need to perform the measurements in the metallographic planes that are inclined with respect to the chosen vertical axis). Nonetheless, the frequency of the angular orientations of the lines in the vertical planes is not equal to that in the 3-D space, and therefore it is essential to correct for this bias, when the intersection counts are performed only in the vertical planes. Baddeley et al. (Ref 9) showed that this bias can be eliminated if the intersection counts are performed using cycloid shape test lines (see Fig. 10) that are oriented such that the cycloid minor axis is parallel to the vertical axis. In such a case, the following equation (Ref 9) can be used for an unbiased estimation of S_V:

$$S_V = 2\langle C_L \rangle \quad \text{(Eq 8)}$$

where $\langle C_L \rangle$ is the population average value of the number of intersections between the cycloid shape test lines and the microstructural surfaces of interest per unit test line length, when the cycloids are placed in the vertical sections with their minor axis parallel to the vertical axis. Figure 11 illustrates such intersection counting using cycloid test lines.

Numerous materials processes lead to the microstructural anisotropy that has a natural rotational symmetry axis. For example, the morphological anisotropy of the grain boundaries in an extruded (or wire drawn) polycrystalline metal is rotationally symmetric with respect to the extrusion direction (wire axis). In such a material, all the metallographic planes containing the symmetry axis present statistically similar 2-D microstructures. Therefore, if the symmetry axis is chosen as the vertical axis, then all the corresponding vertical planes yield statistically similar intersection counts. Consequently, in such homogenous anisotropic microstructures, S_V can be estimated by performing the intersection counts using cycloid shape test lines placed in a single vertical plane containing the symmetry axis (vertical axis) using Eq 8. Thus, the methodology developed by Baddeley and coworkers (Ref 9) provides a very efficient practical solution for the estimation of S_V in the anisotropic microstructures that have a symmetry axis.

Several materials processes lead to the microstructural anisotropy that does not have a rotational symmetry axis. For example, the morphological anisotropy of the grain boundaries in a cold-rolled metal is not rotationally symmetric with respect to the rolling direction (or with respect to any other direction). In such cases, Eq 8 is still applicable, but the measurements must be performed on vertical planes of numerous different orientations. Further, it is not known a

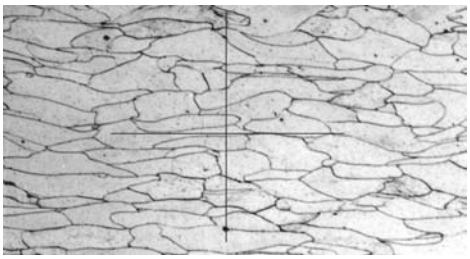

Fig. 7 Anisotropic microstructure of a specimen of cold rolled extra-low-carbon steel, where the number of intersections between a test line and grain boundaries strongly depends on the angular orientation of the test line. For example, in this microstructure, a vertical test line is expected to intersect a significantly higher number of grain boundaries than a horizontal test line of the same length.

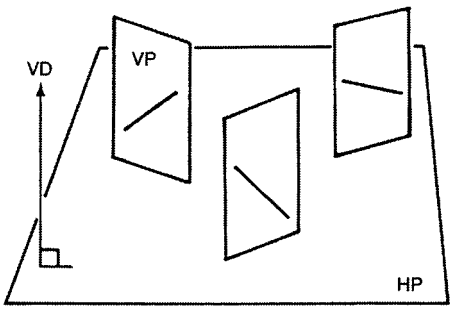

Fig. 8 Concept of vertical direction/axis (VD) and vertical planes (VP). HP is horizontal plane. Source: Ref 9

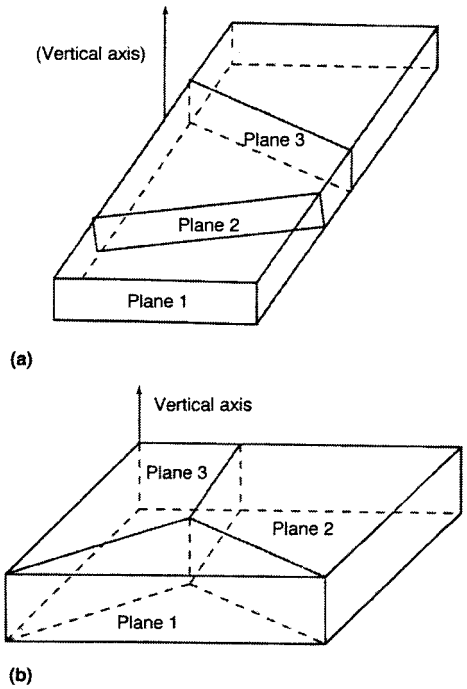

Fig. 9 Vertical planes. (a) At different locations in the specimen. (b) At the same location in the specimen

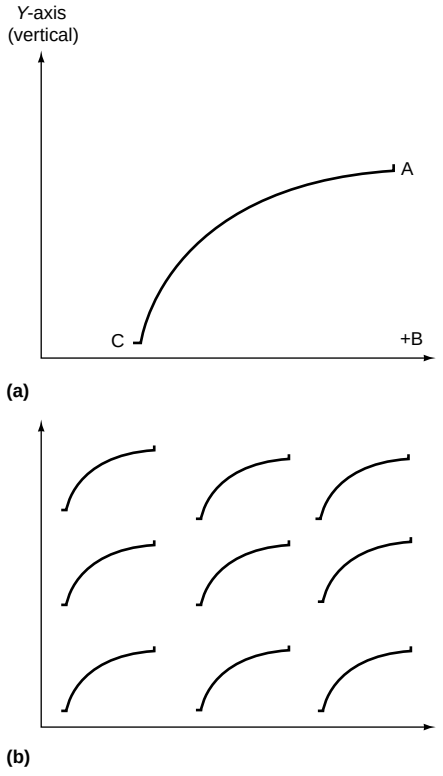

Fig. 10 Cycloid shape test lines. (a) Cycloid curve oriented with its minor axis (AB) parallel to the *Y*-axis (vertical axis). The length of the cycloid curve is equal to two times the length of its minor axis (AB). Parametric equation of cycloid is $Y = 1 - \cos\theta$ and $X = \theta - \sin\theta$. The parameter θ takes values from 0 to π. (b) A measurement grid containing nine cycloids. For the surface area measurements the grid must be oriented so that the arrow is parallel to the vertical axis.

priori on vertical planes of how many different orientations the measurement need to be performed for a reliable estimation of S_V, because the answer depends on the morphological orientation distribution function of the surfaces of interest (which is usually unknown). This problem has been analyzed by Gokhale and Drury (Ref 10) using theoretical analysis and computer simulations. It has been shown that the measurements on vertical planes of at the most three orientations are always sufficient for an estimation of S_V with a bias of less than 5% in a microstructure of any arbitrary anisotropy, if the sampling and the intersection counts are performed using a trisector probe (which consists of three vertical planes) using the following procedure (Ref 10):

1. The vertical axis should be chosen such that it is *not* parallel to most of the surfaces of interest. For example, in a cold-rolled plate or sheet, the thickness direction can serve as such vertical axis.
2. The first vertical plane (obviously, it must contain the chosen vertical axis) is chosen in a completely arbitrary fashion.
3. The second and the third vertical planes of the trisector are chosen such that they are at an angle of 120° to the first vertical plane and to one another. This yields a set of three vertical planes that are mutually at angle of 120° and contain a common direction that is the chosen vertical axis (see Fig. 12). The three planes of the trisector need not be at the same location in microstructure, and to optimize the efficiency and to minimize the bias, they should not be at the same location.
4. On each vertical plane of the trisector, place a set of cycloid shape test lines and sample the plane in a systematic manner. The cycloid minor axis must be parallel to the vertical axis.
5. Count the number of intersections between the cycloid test lines and the microstructural surfaces of interest, and calculate the average number of intersections per unit test line length (see Fig. 11 for an illustration of the counting procedure).

The total surface area per unit volume S_V can be then estimated using a stereological equation (Ref 10):

$$S_V = 2\langle T_L \rangle \quad \text{(Eq 9)}$$

where $\langle T_L \rangle$ is the population average value of the number of intersections of the microstructural surfaces with the cycloid shape test lines in the trisector planes per unit test line length. Note that Eq 6, 8, and 9 are formally identical: they differ only in the sampling procedures used for the intersection counting. The trisector technique has been used in several recent studies for estimation of S_V in anisotropic microstructures (Ref 10, 11, 17, 55, 56, 62–64).

Figure 13 shows a plot of the total surface area of the grain boundaries per unit volume estimated using the trisector technique versus the amount of cold work in a set of specimens of cold-rolled extra-low-carbon steel (Ref 11). In these specimens, the initial microstructure before the cold rolling was the same. The data show that the total grain boundary area increases with amount of cold work. Therefore, the plastic deformation creates new grain boundary surfaces.

Estimation of Total Projected Surface Area per Unit Volume

In the microstructure-properties correlation studies involving anisotropic microstructures, another microstructural parameter of interest is the total projected surface area of the microstructural surfaces of interest on a plane of specific angular orientation (θ, ϕ) per unit volume, $A_V(\theta, \phi)$. This parameter can also be estimated in a straightforward manner. Let $\langle I_L(\theta, \phi) \rangle$ be the average number of intersections between straight

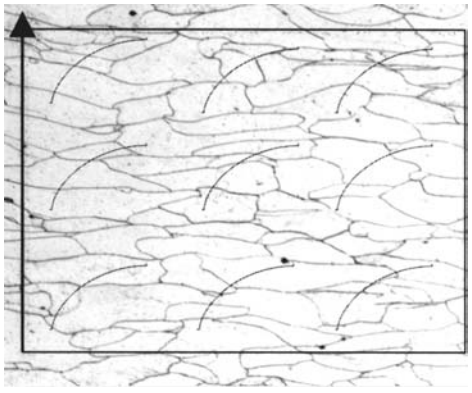

Fig. 11 A set of nine cycloid test lines superimposed on the microstructure observed in a vertical metallographic plane of a specimen of cold rolled extra-low-carbon steel (Ref 11). In this case, the chosen vertical axis (*Y*-axis) is the direction perpendicular to the faces of the rolled plate. The number of intersections between these nine test lines and the anisotropic grain boundaries is equal to 36. The effective length of cycloid minor axis was 138 μm. The length of a cycloid arc is two times the length of its minor axis. Therefore, the number of intersections per unit test line length is equal to $[36]/\{9 \times (2 \times 138)\} = 0.0145$ per μm.

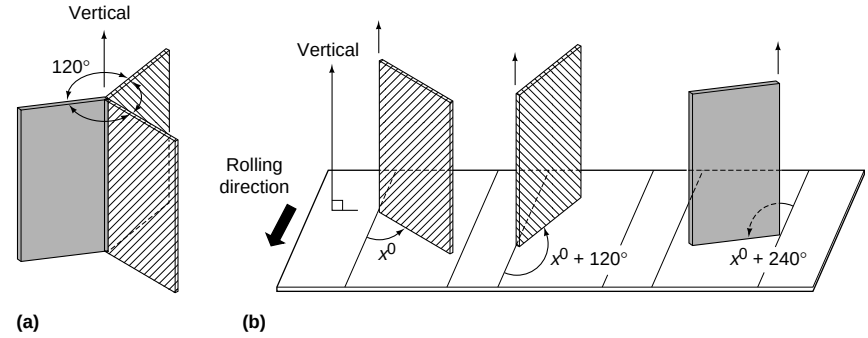

Fig. 12 Use of a trisector probe. (a) The trisector consists of three vertical planes that are mutually at an angle of 120° where the vertical axis is not parallel to most of the surfaces of interest. (b) In a rolled metal plate, most of the grain boundaries are parallel to the rolling directions, and therefore the vertical axis of the trisector can be the direction perpendicular to the faces of the plate. For the trisector sampling, the angular orientation x^0 of the first vertical planes is chosen at random. The orientations of the remaining two planes are obtained by adding 120° and 240°, respectively, to the first one. The three planes of the trisector need not be at the same location. Source: Ref 10, 64

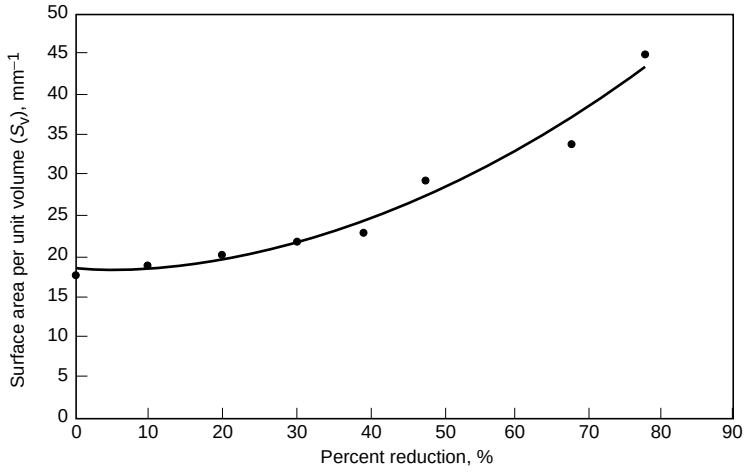

Fig. 13 Plot of total surface area of the grain boundaries per unit volume measured using the trisector technique versus the amount of cold work in a set of specimens of cold-rolled extra-low-carbon steel. Source: Ref 11

test lines of orientation (θ, ϕ) and the microstructural surfaces per unit test line length. It can be shown that (Ref 6–8, 61):

$$A_V(\theta, \phi) = \langle I_L(\theta, \phi)\rangle \quad \text{(Eq 10)}$$

In other words, the intersection counts using straight test line of specific angular orientation essentially represent the total projected area of the surfaces on a plane perpendicular to the direction of the test lines. Figure 14 shows a plot of plane strain fracture toughness K_{Ic} versus the total projected area of the high angle grain boundaries between recrystallized and unrecrystallized regions on the plane perpendicular to the loading direction, in a set of specimens of partially recrystallized hot-rolled 7050 aluminum alloy having different degrees of recrystallization and orientations (Ref 55). The K_{Ic} decreases with the increase in the projected area of the boundaries indicating that these boundaries adversely affect the fracture toughness of the alloy.

Estimation of Sampling Error. To estimate the sampling error in the total surface area per unit volume S_V, let L_T be the total effective length of the set of test lines used for the intersection counting. Suppose that these test lines are placed in n number of fields of view, and the intersections between the test lines and the surfaces of interest are counted. Let I_1, I_2, . . ., I_i, . . . I_n represent these intersection count data, which essentially constitute a statistical sample of size n. In this sample, the average number of intersections $\langle I\rangle$, that is, the sample average, is given as:

$$\langle I\rangle = \Sigma I_i/n \quad \text{(Eq 11)}$$

If the sample size is sufficiently large (for most microstructures, $n > 50$), then the following working equation gives the confidence interval in the S_V estimated from the experimental intersection counts data:

$$E_n = 4\{\Sigma(\langle I\rangle - I_i)^2/[n(n-1)(L_T)^2]\}^{1/2} \quad \text{(Eq 12a)}$$

$$S_V = [2\langle I\rangle/L_T] \pm E_n \quad \text{(Eq 12b)}$$

Equation 12(b) implies that there is 95% probability that the true value of the total surface area per unit volume S_V is in the interval $\{2[\langle I\rangle/L_T] \pm E_n\}$. Note that the sampling error E_n strongly depends on the sample size n, and therefore it can be kept as small as desired by simply increasing the sample size n, that is, number of microstructural fields on which the measurements are performed. If the sample size is not sufficiently large (i.e., $n < 50$) then other statistical procedures must be used to compute the confidence interval (Ref 75). Note that Eq 12(a) and (b) are applicable for calculation of confidence interval when the intersection counts are performed by using straight test lines, or by using cycloid shape test lines.

Total Length per Unit Volume

One-dimensional lineal features are usually present in material microstructures. Dislocation lines, grain edges, triple lines, and necks in the sintered microstructures are examples of the microstructural features that are truly one-dimensional. Further, the features such as needle-shaped precipitates, whiskers in composites, slag stringers, and so forth can be modeled as one-dimensional lineal features. An important attribute of the lineal microstructural features is their total length per unit volume, or so-called length density. Numerous material properties depend on the length density of the lineal features present in microstructure. For example, almost all the plastic-deformation-related mechanical properties of crystalline materials depend on the dislocation density. The total line length per unit volume is denoted by the symbol L_V. It is equal to the sum of the lengths of the lineal features of interest in a specimen divided by the specimen volume. In the symbol L_V, the subscript V signifies the normalization with the specimen volume. The units of L_V are $\mu m/\mu m^3$ or $(\mu m)^{-2}$. Since L_V is not dimensionless, it is necessary to know the microscope magnification for its estimation. The length density can be estimated from the measurements performed in the metallographic planes, or in the projected images of a 3-D microstructure. These two techniques are described in the paragraphs that follow.

Estimation of L_V from Measurements Performed in Metallographic Planes. The 2-D metallographic planes serve as geometric probes for the estimation of L_V. The intersections of lineal features with a metallographic plane result in "points." These points can be observed in a metallographic plane. For example, the triple junctions in Fig. 15(a) are the intersections of the grain edges with the metallographic plane. One can count the number of such points per unit area of the metallographic plane, Q_A. The population average value of number of points per unit area $\langle Q_A\rangle$ is related to the length density of the lineal features as follows (Ref 8, 61):

$$L_V = 2\langle Q_A\rangle \quad \text{(Eq 13)}$$

Note that $\langle Q_A\rangle$ has units of $(\mu m)^{-2}$. The triple-point counting procedure is illustrated in Fig. 15. For isotropic microstructures, it is not necessary to randomize the angular orientation of the metallographic plane. In such a case, the measurements in the metallographic planes of any one convenient orientation can give a reliable estimate of L_V. If the microstructure is isotropic and homogeneous (i.e., no gradients), then the measurements performed in a single metallographic plane of any one angular orientation and at any convenient location in the specimen should yield a reliable estimate of L_V. For most homogeneous isotropic material microstructures, measurements on about 50 to 60 uniformly distributed microstructural fields can yield a reliable estimate of L_V.

In an anisotropic microstructure, Q_A varies systematically with the angular orientation of the metallographic plane. Consequently, it is essential to perform the measurements on numerous metallographic planes of different random angular orientations to obtain a reliable estimate of the population average $\langle Q_A\rangle$. At present, no stereological technique is available for efficient estimation of the length density in an anisotropic microstructure from the measurements performed on few metallographic planes. However, an efficient stereological technique for the estimation of the length density in any anisotropic microstructure is available if the measurements can be performed on the projected images of the microstructure. This alternate method is described below.

Estimation of L_V from Measurements Performed in Projected Images. For numerous

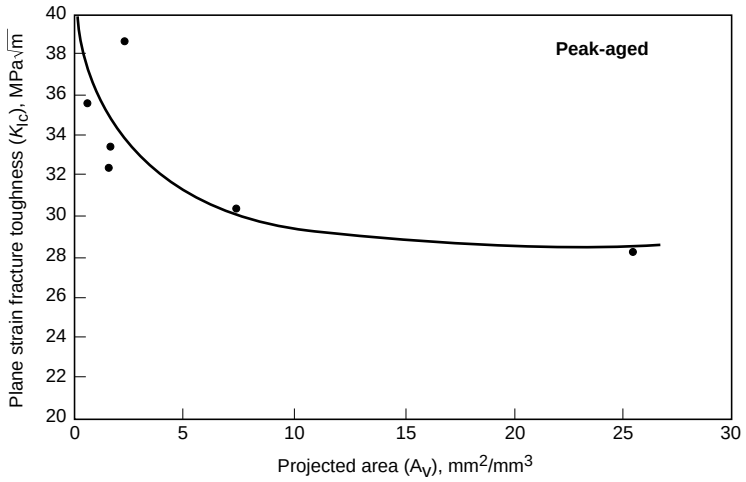

Fig. 14 Plot of plane strain fracture toughness K_{Ic} versus the total projected area of the high-angle grain boundaries between recrystallized and unrecrystallized regions per unit volume A_V on the plane perpendicular to the loading direction in a set of specimens of partially recrystallized hot-rolled 7050 aluminum alloy having different degrees of recrystallization and orientations. Source: Ref 55

microstructures, transmission microscopy (for example, transmission electron microscopy, radiography, and so forth) is the microscopy technique of choice. In such cases, efficient estimation of the length density of lineal features from the projected microstructural images is of particular interest. This design-based stereological method involves vertical slices sampling procedure developed by Gokhale (Ref 13–15):

1. Choose a convenient reference direction in the 3-D space. This reference direction is called vertical axis.
2. A slice is a microstructural volume contained between two parallel planes that are separated by distance, Δ, which is the thickness of the slice. A vertical slice is a slice whose parallel faces contain the chosen vertical axis (see Fig. 16). Uniformly sample the 3-D microstructure with vertical slices.
3. Observe the projected images of the lineal features contained in the vertical slices (Fig. 17).
4. Place cycloid shape test lines on the projected images of the vertical slices such that the cycloid minor axis is perpendicular to the vertical axis. Such test lines essentially represent the projections of hypothetical cycloidal test surfaces in the vertical slices as illustrated in Fig. 17.
5. Count the number of intersections between the cycloid shape test lines and the projected images of the lineal features of interest, and calculate the number of intersections per unit length (see Fig. 18).

The population average value of this quantity $\langle J_L \rangle$ is related to the length density L_V through the stereological equation (Ref 13–15):

$$L_V = 2\langle J_L \rangle / \Delta \qquad \text{(Eq 14)}$$

This result has been utilized to estimate the length density of anisotropic lineal biological features in numerous biological tissues (Ref 65–68); the technique is equally applicable for the estimation of dislocation density from transmission electron microscopy (TEM) images.

If the anisotropy of the lineal features of interest has a natural rotational symmetry axis, then the projected images of all the vertical slices containing the symmetry axis present statistically similar projected microstructures. Therefore, if the symmetry axis is chosen as the vertical axis, then all the corresponding vertical slices yield statistically similar intersection counts. Consequently, in such anisotropic microstructures, L_V can be estimated by performing intersection counts on the projected images of vertical slices of just one orientation containing the symmetry axis (vertical axis). If the anisotropy of the lineal features does not have a natural symmetry axis, then sampling similar to the trisector consisting of three vertical slices mutually at an angle of 120° yields a reliable estimate of L_V, if the vertical axis is not parallel to most of the lineal features (Ref 69).

Estimation of Sampling Error. For computation of the sampling error in the estimated total length per unit volume L_V from the measurements performed in the metallographic planes, let A_T be the total effective area of the measurement frame used for counting. Suppose this measurement frame is placed in n number of fields of view, and the intersections between the frame and the lineal features of interest are counted. Let $Q_1, Q_2, \ldots, Q_i, \ldots Q_n$ represent these data, which essentially constitute a statistical sample of size n. In this sample, the average number of intersections $\langle Q \rangle$; that is, the sample average, is given as:

$$\langle Q \rangle = \Sigma Q_i / n \qquad \text{(Eq 15)}$$

If the sample size is sufficiently large (for most microstructures, $n > 50$) then the L_V estimated

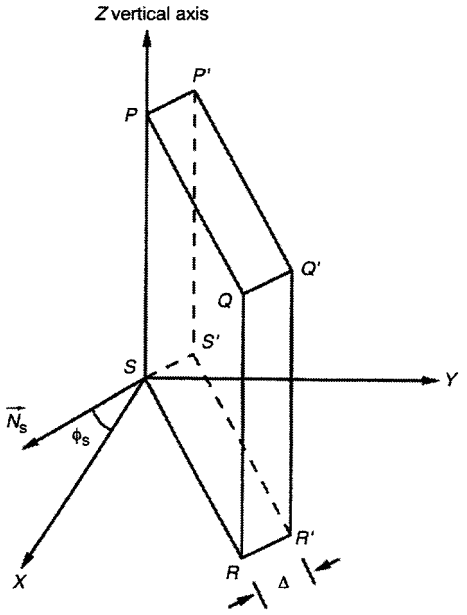

Fig. 16 Concept of vertical slice. A vertical slice is any microstructural volume contained between two vertical planes (faces of the slice) separated by distance, Δ, which is the slice thickness. Source: Ref 13, 14

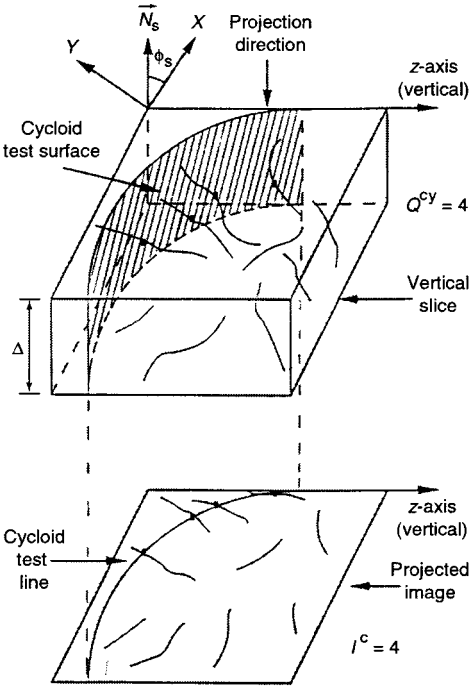

Fig. 17 A cycloid placed in the projected image of a vertical slice can be treated as projected image of hypothetical cycloidal surface contained in the slice. The number of intersections Q between the lineal features of interest in the slice and such cycloidal surface is exactly equal to the number of intersections I between the corresponding cycloid in the projected image and the projected images of the lineal features. Source: Ref 13

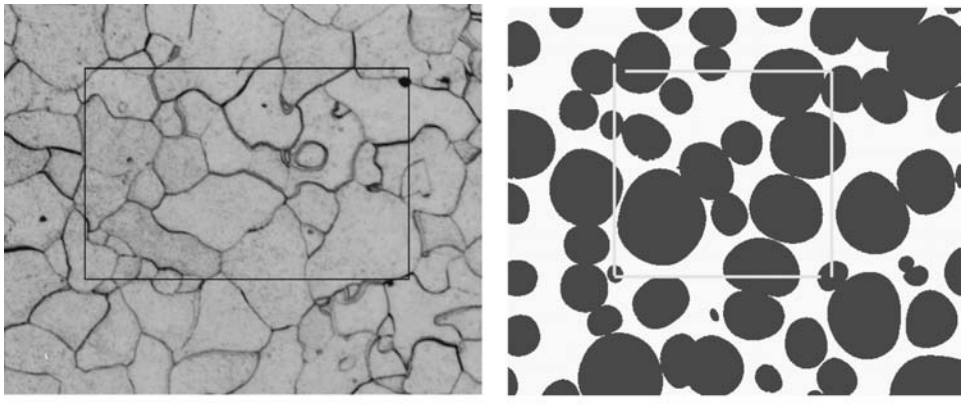

Fig. 15 Triple-point counting procedure. (a) Microstructure of well-annealed extra-low-carbon steel containing equiaxed grains. The triple junction points (i.e., junctions of three grain boundary traces) are points of intersections of grain edges in the 3-D microstructure with the metallographic plane. In the measurement frame there are 45 triple junction points in the measurement frame having the effective area of 36.5×10^4 μm^2. Therefore, Q_A is equal to $45/[36.5 \times 10^4] = 1.23 \times 10^{-4}$ per μm^2. (b) Microstructure of liquid phase sintered tungsten heavy alloy depicting tungsten grains. The "necks" are the loops that bound the grain boundary between each pair of abutting tungsten grains in the 3-D microstructure. The intersections of these necks with the metallographic plane yield solid-solid-liquid triple junction points (i.e., common junction points of two tungsten grains and matrix). In the measurement frame, there are 16 such triple junction points, and the frame has effective area of 10^4 μm^2. Therefore, Q_A is equal to $16/[10^4] = 1.6 \times 10^{-3}$ per μm^2.

from this sample and the associated confidence interval are given as:

$$L_V = 2[\langle Q\rangle/A_T] \pm E_n \quad \text{(Eq 16)}$$

$$E_n = 4\{\Sigma(\langle Q\rangle - Q_i)^2/[n(n-1)(A_T)^2]\}^{1/2} \quad \text{(Eq 17)}$$

Equation 16 states that there is 95% probability that the true value of the total length per unit volume is within the interval given by the right-hand side of the equation. As mentioned earlier, other statistical procedures need to be used for small samples (Ref 75).

Number Density of Microstructural Features (How Many?)

Number density of a given type of microstructural features (for example, voids, particles, grains) is equal to the average value of the number of such features per unit microstructural volume. This is an important microstructural parameter of interest in processing-microstructure-properties studies. Unfortunately, in general, the number density of the features in a 3-D microstructure cannot be estimated from any measurements performed on independent 2-D metallographic sections, unless the particles/grains have a known simple convex shape (Ref 2, 6–8). Consequently, in the past, reliable estimation of number density was problematic. In 1984, Sterio (Ref 19) showed that the number density of the features in a 3-D microstructure can be estimated using a test probe (called disector) consisting of two parallel metallographic planes that are a small distance apart (i.e., two closely spaced serial sections). In 2000 (Ref 20), a combination of this sampling principle and modern image analysis techniques led to an efficient stereological method for an unbiased and efficient estimation of the number density from the measurements performed on the digital images of two closely spaced large-area high-resolution montage serial sections, called large-area disector (LAD). To understand these 3-D techniques, first an unbiased method for counting particles/grains in a 2-D metallographic plane is presented, and then the estimation of the number density in the 3-D microstructures is described.

Estimation of Number of Particles/Grains per Unit Area in a Metallographic Plane. In any microscope, a limited area of the metallographic plane is observed in one field of view. Therefore, there are usually some features that cross the boundaries of the field of view (or measurement frame), which can lead to a counting bias due to an "edge effect." This is because such partly-in-partly-out features raise the question whether to include them in the number count, to exclude them, or to count them as one-half. Gundersen (Ref 76) has shown that none of these is a statistically unbiased and correct procedure. The correct statistical procedure to account for the edge effect requires the use of an unbiased counting frame (Ref 76). An unbiased counting frame consists of a square measurement frame of area A_f that has two forbidden edges (solid lines in Fig. 19), and two permissible edges (dashed lines in Fig. 19). The counting procedure is:

1. Count all the features that are completely contained in the measurement frame and therefore do not intersect any edges of the counting frame.
2. Do not count any feature that intersects a forbidden edge.
3. Count all the features that intersect the permissible edge(s), if they do not also intersect any forbidden edge.
4. The average value of the number of features counted in this manner divided by the area of the measurement frame A_f is an unbiased estimator of the two-dimensional number density of the features of interest in the metallographic plane.

This procedure for unbiased counting of the number of features in a metallographic section is shown in Fig. 19.

Disector Principle for Unbiased Estimation of Number Density in 3-D Microstructure. Sterio (Ref 19) has developed a three-dimensional stereological sampling probe, disector, for an unbiased estimation of the number density of the features of interest in any three-dimensional microstructure. The disector consists of two parallel metallographic planes (i.e., two serial sections) that are separated by a known distance *t*. The distance *t* between the disector planes must be less than one-fifth of the average size of the features of interest. Observations on both the planes of the disector are required for the estimation of the number density. An unbiased counting frame of area A_f is placed in the first disector plane to sample the features of interest using the counting procedure described in the previous subsection (and shown in Fig. 19), and these features are followed in the second plane. Out of the features sampled by the unbiased counting frame in the first disector plane, those that are not present in the second plane, Q^-, are counted. The average value of the quantity $[Q^-]/[A_f t]$ is an unbiased estimator of number of features per unit volume (i.e., number density) N_V in the three-dimensional microstructure. Alternately, an unbiased counting frame can be placed in the second metallographic plane of the disector, and the features sampled by the unbiased frame that are not present in the first plane, Q^+, may be counted in exactly the same way. In practice, it is efficient to count both Q^+ and Q^- and use the following equation for an unbiased estimation of the number density, N_V (Ref 19):

$$N_V = [Q^+ + Q^-]/[2A_f t] \quad \text{(Eq 18)}$$

The disector procedure is shown in Fig. 20. In the opaque material microstructures, a practical application of the disector probe requires storing of an image (or a micrograph) of a field of view in the first disector plane, physical removal of small known thickness of the specimen by polishing, followed by suitable etching to reveal microstructure, and the observations in the second sectioning plane to determine how many features sampled by the unbiased counting frame placed in the field of view in the first plane are not present in the second sectioning plane. In this process, the least amount of effort is required for the

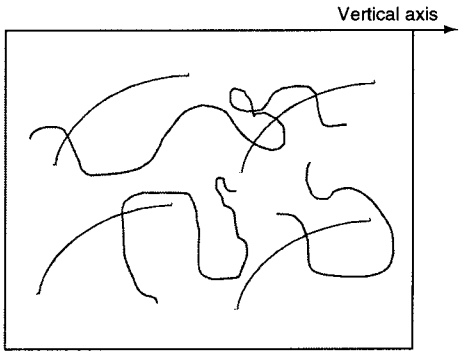

Fig. 18 Four cycloid shape test lines superimposed on the projected image of a vertical slice containing lineal features. Note that, for the length estimation, the cycloid minor axis must be perpendicular to the vertical axis. In this example, there are a total of six intersections between the four cycloid test lines and the projected images of the lineal features. For the cycloids having minor axis equal to 20 μm, the length of each test line would be 40 μm, and J_L would be equal to $6/[4 \times 40] = 0.0375$ per μm.

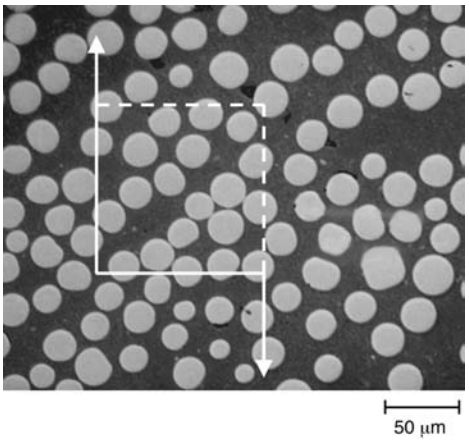

Fig. 19 Microstructure of a ceramic-matrix composite containing unidirectional continuous nicalon (SiC) fibers in MAS glass ceramic matrix observed in a transverse metallographic plane. An unbiased square counting frame consisting of two forbidden edges (solid line) and two permissible edges (dashed lines) is overlaid on the microstructure. There are 11 fibers completely inside the counting frame; there are nine fibers that intersect one or both forbidden edges (therefore, not to be included in the number count); and there are five fibers that intersect one or both permissible edges but do not intersect any forbidden edge (therefore, to be included in the number count). Thus, effectively there are 16 fibers in the measurement frame of area 3953 μm^2. Thus, the local value of the number of fiber per unit area is equal to 4.05×10^{-3} per μm^2.

actual stereological counting; most of the effort (about 90%) goes into the specimen preparation steps such as physical sectioning, polishing, etching of disector planes, identification of the same microstructural region in the two sectioning planes, alignment of the images in the two planes, and measurement of thickness (i.e., distance between disector planes) of the material removed. After all the tedious metallographic work, very small numbers of particle counts are obtained. The number density estimated from such a small statistical sample (although unbiased) has a large sampling error. Therefore, to obtain a reasonably precise estimate of the number density and to decrease the sampling error, it is necessary to repeat the procedure on (typically) 25 to 50 different disectors, which requires physical sectioning of a large number of metallographic planes and involves tedious metallographic work. A practical solution to this problem has been recently developed (Ref 20) that utilizes a combination of the disector principle and modern digital image processing techniques; the resulting sampling technique, called large-area disector (LAD), is described below.

Large Area Disector (LAD) for Efficient and Unbiased Estimation of Number Density. The major limitation of the conventional disector technique is that it is inefficient for the estimation of the number density in opaque material microstructures due to low Q^+ and Q^- counts usually obtained from a disector whose area is equal to one field of view. The counts can be increased by increasing the absolute area of the field of view selected in the first sectioning plane simply by observing the structure at a much lower magnification. This is often not acceptable because the loss of resolution can lead to significant measurement errors. In almost all microscopy techniques, to obtain a higher resolution the structure must be observed at a higher magnification, and that decreases the area of the observed microstructural field of view. Therefore, it is not possible to observe a large area of a metallographic plane at a high resolution using the conventional microscopy techniques. However, it is possible to obtain a large microstructural area at a high resolution by creating a "seamless montage" of a very large number of contiguous microstructural fields grabbed at a high resolution and "stitched together" using the digital image analysis procedure given elsewhere (Ref 22, 23, 35). Using such a methodology, the number density can be efficiently estimated:

1. Identify a sufficiently large region in the first disector plane covering about 25 to 100 microstructural fields, and "tag" this region by placing sufficient number of deep microhardness indents around its four boundaries.
2. Create a seamless "montage" covering all the microstructural fields in this region of the first disector plane at sufficiently high resolution such that all the features of interest are clearly resolved, using the "montage" image analysis technique described in detail in Ref 22, 23, and 35. Figure 21 illustrates one such large-area-high-resolution montage.
3. Remove a small amount of material by polishing and identify the same region in the second disector plane by using the positions of the microhardness indents for reference.
4. Create the seamless montage of all the microstructural fields of the same region in the second disector plane, and align the two montages using the micro-hardness indents as the reference points (Ref 20). The two montages then constitute the LAD (see Fig. 22).
5. Measure the disector thickness t by measuring the decrease in the sizes of microhardness indents in the second disector plane (Fig. 23).
6. Place a large unbiased counting frame in the first LAD plane and note the features that can be effectively assigned to that frame using the unbiased counting procedure given by Sterio (Ref 19).
7. Out of the features sampled by the first plane of the LAD, identify the number of features that are absent in the second plane (i.e., Q^-), or vice versa (i.e., Q^+), as illustrated in Fig. 20, and estimate the number density using Eq 18.

In the uniform random microstructures (i.e., no gradients), a reliable and precise estimation of the three-dimensional number density of the particles (or any other features of interest) can be made by systematically sampling with three LADs at three different systematic random locations (Ref 20). The LAD sampling has been successfully used to estimate the 3-D number

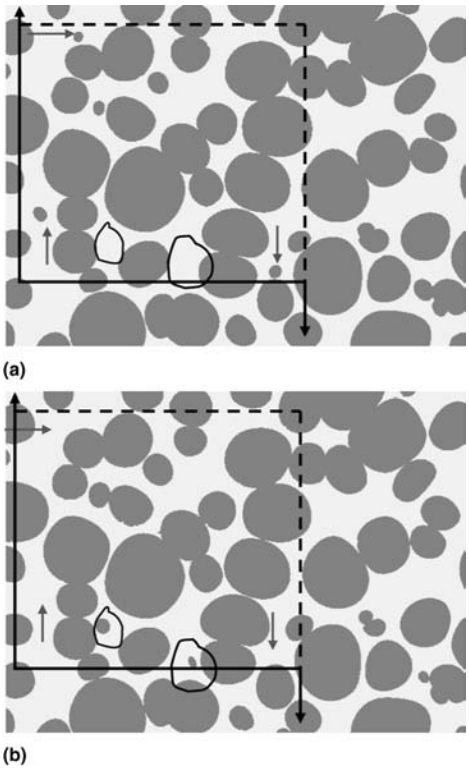

Fig. 20 Disector sampling method for estimation of number density of tungsten grains in the 3-D microstructure of liquid phase sintered W-Ni-Fe alloy. The three grains in (a) at the arrows are sampled by the unbiased counting frame, which are not present in the second disector plane segment shown in (b). Therefore, Q^- is equal to 3. On the other hand, the two grains that are circled in (b) are not present in (a). Therefore, Q^+ is equal to 2. The area of the sampling frame is 2×10^5 μm^2. In this case, the distance between the two disector planes was 1 μm. Thus, using Eq 18, the estimate of number density of tungsten grains N_V is $[2 + 3]/[(2 \times 10^5) \times 1\} = 2.5 \times 10^{-5}$ per μm^3 of microstructural volume. Source: Ref 20

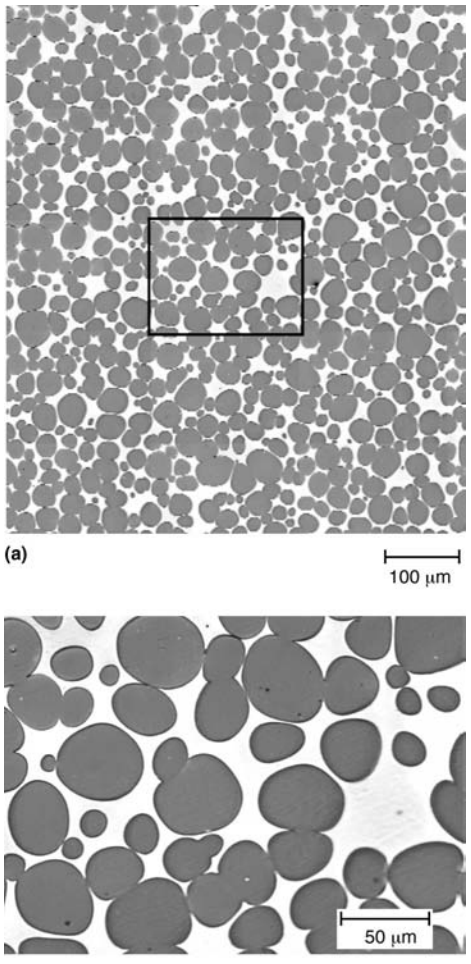

Fig. 21 Microstructure of liquid phase sintered W-Ni-Fe alloy containing tungsten grains (dark) in nickel-iron alloy matrix. (a) Seamless montage of a large number of contiguous microstructural fields grabbed at high resolution and then digitally compressed for presentation. Each field of the montage was grabbed at a magnification and resolution of the field of view shown in (b), which is the central bordered microstructural field in the compressed montage. Source: Ref 20

density of tungsten grains in a liquid phase sintered W-Ni-Fe alloy processed in normal gravity and microgravity (Ref 20) and the 3-D particle cracking damage in some wrought aluminum alloys as a function of strain under uniaxial tension and compression (Ref 43, 58).

Derived Microstructural Properties

Derived microstructural properties such as grain size, mean free path, and mean particle volume often appear as parameters in the models and theories of materials behavior. These attributes can be computed from experimentally measured numerical extents and number densities of the microstructural features of interest, and therefore they are not independent microstructural characteristics. Nonetheless, they are extremely useful for understanding microstructure-properties interrelationships, and consequently these microstructural parameters are used in many studies (Ref 11, 43, 47, 49, 52, 58–60 77–80). Important derived microstructural properties are described in the paragraphs that follow.

Mean Free Path. The average uninterrupted surface-to-surface distance between precipitates (or regions of any phase of interest) through the matrix in a three-dimensional microstructure is called mean free path (see Fig. 24). The mean free path is denoted by the symbol, $\langle\lambda\rangle$. Numerous mechanical properties (for example, yield stress) of microstructures containing a population of precipitates depend significantly on the mean free path of the precipitates. The mean free path $\langle\lambda\rangle$ is related to the volume fraction of precipitates, V_V, and their total surface area per unit volume, S_V through (Ref 81, 82):

$$\langle\lambda\rangle = 4[1 - V_V]/S_V \quad \text{(Eq 19)}$$

Equation 19 is applicable to any arbitrary microstructure containing precipitates or particles or inclusions: it does not involve any assumptions. The microstructure need not be isotropic; and all the particles need not be of the same size or shape. The mean free path is also a measure of the length scale of a microstructure, and it has been used in numerous studies to correlate the microstructure to the material properties, as well as to monitor microstructural evolution processes. For example, this parameter has been utilized to monitor devitrification and microstructural coarsening in some aluminosilicate glasses (Ref 47).

Mean Free Path along a Specific Direction. In an isotropic microstructure, the average free path is the same along all the directions in the three-dimensional microstructural space. However, in an anisotropic microstructure, the average free path varies with the direction, and therefore, average free path along a specific direction (for example, rolling direction in a cold-rolled steel) may be of interest. The average free path through the matrix $\lambda(\theta, \phi)$ along the direction having the orientation (θ, ϕ) can be computed by using the general stereological equation:

$$\lambda(\theta, \phi) = 2(1 - V_V)/I_L(\theta, \phi) \quad \text{(Eq 20)}$$

where $I_L(\theta, \phi)$ is the average number of intersections between the particle matrix interfaces and the straight test lines of orientation (θ, ϕ) per unit length.

Grain Size. The mean intercept grain size in a single-phase polycrystalline material, G, is equal to the average length of the chords formed by intersections of the grains with random straight test lines. The mean intercept grain size G can be computed using:

$$G = 1/\langle I_L\rangle \quad \text{(Eq 21)}$$

where $\langle I_L\rangle$ is the average number of intersections between the test lines and the grain boundaries per unit test line length. Combining Eq 6 and 21 gives:

$$G = 2/S_V \quad \text{(Eq 22)}$$

where S_V is the total area of the grain boundaries per unit volume of the material. The ASTM grain size number n can be calculated from G by using the following equation given in ASTM E 112 (Ref 83):

$$n = [-6.644 \log G] - 3.288 \quad \text{(Eq 23)}$$

where the mean intercept grain size G is expressed in the units of millimeters.

Combining Eq 22 and 23 gives:

$$n = 6.644 \log S_V - 5.288 \quad \text{(Eq 24)}$$

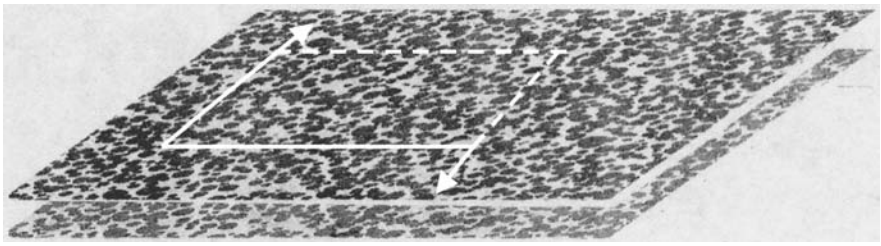

Fig. 22 Two planes of large-area disector (LAD), each of which is a seamless montage of large number of contiguous microstructural fields grabbed at a high resolution. A large area unbiased counting frame is overlaid on the first LAD plane. Source: Ref 20

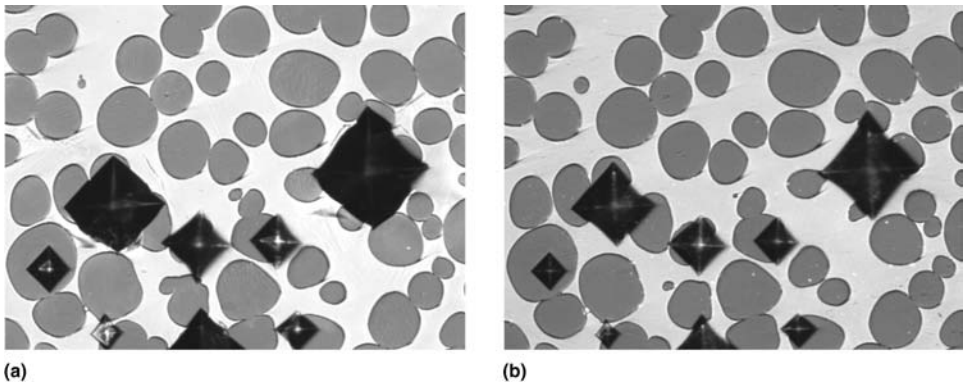

Fig. 23 Use of microhardness indents to measure disector thickness. (a) Microhardness indents placed in the first large-area disector (LAD) plane become smaller in the second LAD plane (b). The change in the size of the indents can be used to compute the amount of material removed (i.e., LAD thickness t), and the locations of the indents can be used to align the two LAD planes. Source: Ref 20

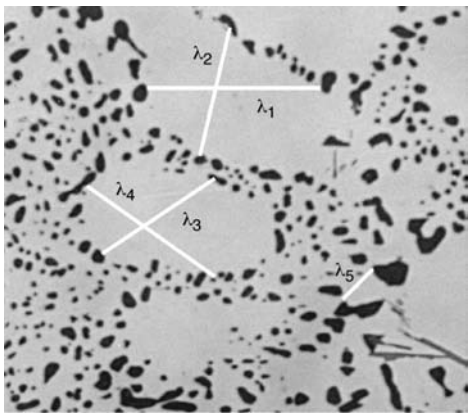

Fig. 24 Microstructure of a cast Al-Si-Mg base alloy containing silicon particles in the interdendritic eutectic regions. The "free path" is an uninterrupted surface-to-surface distance between the particles through the matrix. The distances λ_1 to λ_5 are few examples of such free paths between the silicon particles. The mean free path is the average of obtained by averaging the free path lengths over all locations and all angular orientations.

Therefore, the mean intercept grain size G is inversely proportional to the total surface area of the grain boundaries per unit volume, S_V. Alternately, it can be said that the mean intercept grain size G (and the ASTM grain size number calculated from it) reports the total surface area of the grain boundaries. Figure 25 illustrates the procedure for measurement of mean intercept grain size and ASTM grain size number. The grain size measurement procedures have also been discussed in detail elsewhere (Ref 11, 64, 77, 78, 83).

The mean intercept grain size in an anisotropic microstructure can be also estimated by using Eq 21 and 22. However, $\langle I_L \rangle$ must be obtained by averaging the intersection counts over all angular orientations of the test lines (and metallographic planes), which can be efficiently done by using the trisector methodology (Ref 10, 64) explained earlier. This methodology has been used to characterize the effects of cold rolling on the mean intercept grain size and ASTM grain size number in the microstructure of an extra-low-carbon steel (Ref 11).

ASTM E 112 gives an alternate method for the estimation of grain size number that requires measurement of average number density of grains observed in metallographic sections (i.e., counting the average number of grains per unit area). According to the standard, the ASTM grain size number n can be computed from such data using:

$$n = 1 + 3.3226 \log \langle N \rangle \quad \text{(Eq 25)}$$

where $\langle N \rangle$ is the average number of grains per square inch area of metallographic plane observed at 100× magnification. It is important to recognize that the grain size number calculated from Eq 25 using the 2-D number density of grains and the one calculated from Eq 24 using the intersection counts in the same specimen may not necessarily be equal! This is because the mean intercept grain size (and consequently, the grain size number calculated from such data) is directly related to the total grain boundary area per unit volume S_V, whereas the average number density of grains in metallographic planes (and consequently grain size number calculated from such data, as in Eq 25) is related to the total length of grain edges per unit volume L_V (Ref 84), which is an independent microstructural parameter.

Surface Area Averaged Particle Size. In numerous microstructures, it is of interest to quantify a measure of average particle size. Caliper diameter d of a particle is the distance between two parallel planes tangent to the particle surface at different points. For a sphere, the caliper diameter is equal to the diameter of the sphere, and its value does not depend on the angular orientation of the tangent planes. However, for most of the other shapes (for example, ellipsoid), the caliper diameter varies with the tangent plane orientation. In the case of particles of convex shape, the "average particle size" can be defined as a suitable average value of the caliper diameter. One such measure of average size is the surface area averaged particle size, d_s, where the size is averaged over the surface areas of the particles. The surface area averaged particle size (caliper diameter), d_s is given as (Ref 79):

$$d_s = 6V_V/S_V \quad \text{(Eq 26)}$$

where V_V is the volume fraction and S_V is the total surface area of the particles per unit volume. This equation is applicable to any collection of convex particles; not all the particles need be of the same shape or size, as long as all of them are convex. Further, the microstructure need not be isotropic. It is important to emphasize that, in general, d_S is not equal to the arithmetic average particle size.

Arithmetic Mean Caliper Diameter. The arithmetic mean caliper diameter (average size) of convex particles (or voids, inclusions, etc.) $\langle d \rangle$ can be calculated from experimentally measured three-dimensional number density of particles N_V and the mean value of the number of particles per unit area of sectioning plane $\langle N_A \rangle$ using the following equation given by DeHoff (Ref 7):

$$\langle d \rangle = \langle N_A \rangle / N_V \quad \text{(Eq 27)}$$

Note that in Eq 27, $\langle N_A \rangle$ must be obtained by averaging over the angular orientations of the sectioning planes in 3-D space if the particle has anisotropic (nonrandom) morphological orientations.

Arithmetic Mean Particle Volume. Another measure of average size is the mean particle volume ν. If the number density of particles in the three-dimensional microstructure N_V and their volume fraction V_V are known, then the mean particle volume ν can be computed by using:

$$\nu = V_V/N_V \quad \text{(Eq 28)}$$

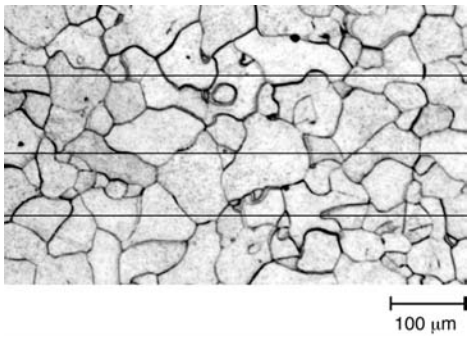

Fig. 25 Microstructure of well-annealed extra-low-carbon steel depicting ferrite grains and grain boundaries. Source: Ref 11. The total number of intersections between the three test lines and the grain boundaries is equal to {10 + 11 + 14} = 35. The total effective length of the test lines is equal to 3.625 mm. Therefore, number of intersections per unit test line length is equal to 9.65 per mm. Mean intercept grain size calculated from these data is equal to {1/9.65} = 0.103 mm (or 103 μm), and the ASTM grain size number calculated using Eq 23 is equal to 3.27.

Similarly, the arithmetic mean particle surface area can be computed from the total surface area per unit volume and number density of the particles.

Contiguity Parameter. In a microstructure containing particles or grains of one phase (e.g., α) in a matrix of another phase (e.g., β), there can be three types of interfaces, namely, αα, ββ, and αβ. The contiguity parameter of the particles, U, is given as (Ref 6, 80).

$$U = 2(S_V)_{\alpha\alpha}/[2(S_V)_{\alpha\alpha} + (S_V)_{\alpha\beta}] \quad \text{(Eq 29)}$$

where $(S_V)_{\alpha\alpha}$ is the total surface area of the αα interfaces per unit volume, and $(S_V)_{\alpha\beta}$ is the total surface area of the αβ interfaces per unit volume. Although, the contiguity parameter is useful for characterization of the extent of particle contiguity, it is not a measure of the topological connectivity of the particles in the 3-D microstructure. The contiguity parameter is frequently used to characterize microstructures of sintered materials (Ref 59, 60).

Dendrite Arm Spacing/Mean Intercepts. Dendrite arm spacing (DAS) is commonly used to characterize cast microstructural fineness. The DAS influences numerous mechanical properties such as strength, fracture toughness, and fatigue life of the cast components. The DAS can be measured in a metallographic section as the mean distance between the dendrite arms, if the dendrite arms are well defined in the observed microstructure (for example as in Fig. 26). Nonetheless, the mean dendrite arm spacing observed in a 2-D section is not necessarily equal to the true mean 3-D arm spacing. It is also important to recognize that a significant operator bias may be introduced in the selection of dendrite arms for the measurement of DAS, and not all cast microstructures containing eutectic constituents have well-defined dendrite arms (for example, see Fig. 27). There are two 3-D stereological parameters of cast microstructures that can be measured in 2-D sections, have a rigorous geometric interpretation, and can equally well characterize cast microstructural fineness: these parameters

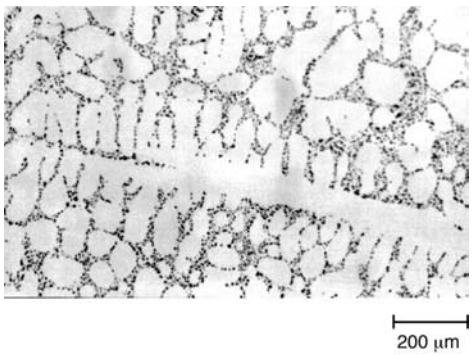

Fig. 26 Microstructure of a cast aluminum-silicon alloy depicting well-developed dendritic structure. The dendrite arm spacing (DAS) is the mean center-to-center distance between the dendrite arms.

are mean linear intercept through dendrites, Ω, and mean intercept through the interdendritic eutectic, ρ. These derived microstructural parameters can be computed:

$$\Omega = 4[1 - (V_V)_e]/(S_V)_e \quad \text{(Eq 30)}$$

$$\rho = 4(V_V)_e/(S_V)_e \quad \text{(Eq 31)}$$

where $(V_V)_e$ is the volume fraction of the interdendritic eutectic and $(S_V)_e$ is the total surface area of between the eutectic and dendrites per unit volume. Note that Ω and/or ρ are not equal to (or directly related to) the DAS, but these attributes provide an alternate measure of the cast microstructural fineness.

Feature-Specific Size, Shape, and Orientation Distributions

Microstructures often contain ensembles of precipitates/inclusions/voids/grains having different sizes, shapes, and morphological orientations. These distributions often evolve during material processing (and/or during service), and they affect material properties and performance. Until recently, most of the stereological techniques for estimation of microstructural distributions were limited to the estimation of the size distributions of randomly oriented geometrically similar particles/voids of simple shapes (for example, spheres, ellipsoids) that differ only in size (Ref 6–8, 12, 85–91). Progress in stereology now enables efficient estimation of true bivariate size-shape (Ref 92) and size-orientation (Ref 38, 45) distributions, as well as trivariate size-shape-orientation distributions of particles/voids (Ref 39) in a three-dimensional microstructure from the measurements performed on few metallographic planes. Nonetheless, all of these techniques do require that the particles/voids of interest be of known convex shape.

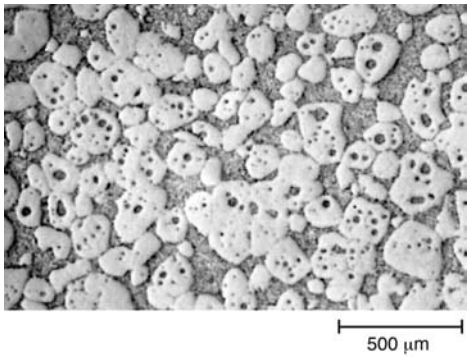

Fig. 27 Microstructure of A356 (Al-Si-Mg base alloy) alloy casting produced by semisolid process. Note that the dendrite cells do not have any well-defined dendrite arms. Therefore, for such cast microstructures, dendrite arm spacing (DAS) does not have any physical meaning. Nonetheless, the microstructural fineness can be still characterized in terms of the stereological parameters such as mean linear intercept of dendrites Ω and mean linear intercept in the interdendritic eutectic ρ.

Size Distribution of Spherical Particles. Numerous stereological procedures have been developed for the estimation of the three-dimensional size distribution of an ensemble of spherical particles in a microstructure from the measurements of the size distribution of the corresponding circular particle sections observed in a representative metallographic plane (Ref 6–8, 12, 85–87, 93, 94). The unfolding technique developed by Saltykov (Ref 8) is the most simple and most frequently used. In this method, the three-dimensional distribution of the sphere diameters is approximated by dividing it into K discrete sizes, where K can be any integer from 7 to 15. The size class interval Δ is defined as:

$$\Delta = D_m/K = d_m/K_m \quad \text{(Eq 32)}$$

where D_m is the diameter of the largest sphere in the three-dimensional microstructure, which is equal to the diameter d_m of the largest circular particle section observed in the metallographic plane. Let $(N_v)_1$, $(N_v)_2$, $(N_v)_3$, . . ., $(N_v)_j$, . . . $(N_v)_K$ be the number of spheres per unit volume having diameters, Δ, 2Δ, 3Δ, . . ., jΔ, . . . KΔ, respectively. The continuous apparent size distribution of the circular particle sections in the metallographic plane is divided into K number of size classes. Let $(n_A)_1$, $(n_A)_2$, $(n_A)_3$, . . ., $(n_A)_i$, . . . $(n_A)_k$ be the number of circles in a two-dimensional metallographic plane per unit area, having the diameters in the size range, (0 to Δ), (Δ to 2Δ), (2Δ to 3Δ), . . ., [(i − 1)Δ to iΔ], . . . [(K − 1)Δ to KΔ], respectively. Saltykov has shown that $(N_v)_j$ are related to $(n_A)_i$:

$$(N_V)_j = \sum_{i=j}^{i=K} b(j, i).(n_A)_i/\Delta \quad \text{(Eq 33)}$$

where $b(j, i)$ are Saltykov's coefficients given in Table 1. Note that the Saltykov's coefficients $b(j, i)$ are negative for $i > j$, they are positive for $i = j$, and there are no coefficients for $i < j$. Therefore, in the summation in Eq 33, all the terms except the first are negative.

For a reliable estimation of the three-dimensional sphere size distribution, it is necessary to measure the diameters of more than 1000 circular particle sections in a metallographic plane, which can be facilitated via automated digital image analysis. The calculation of the sphere size distribution from the section size distribution data using Eq 33 can be done in a straightforward manner using a spreadsheet. As an example, consider Fig. 28(a) depicting gas (air) and shrinkage pores in the microstructure of a high-pressure die-cast AM60 magnesium alloy. The gas pores are round and can be approximated as spheres in the 3-D microstructure, whereas the shrinkage pores are elongated (cracklike) and they form a network that partially connects the gas pores. In this microstructure, to measure the sizes of the round gas pores in the metallographic plane using digital image analysis it is first necessary to separate them from the shrinkage pores, which can be done using an image analysis technique described elsewhere (Ref 28). Figure 28(b) shows the binary image of the field of view shown in Fig. 28(a) that contains only the gas pores because the shrinkage pores have been removed using image processing (Ref 28). The apparent two-dimensional diameter distribution of the gas pores measured from 100 microstructural fields such as Fig. 28(b) is shown in Table 2, and the three-dimensional size distribution of the diameters of the gas pores com-

Table 1 Saltykov's coefficients b (j, i)

	i = 1	i = 2	i = 3	i = 4	i = 5	i = 6	i = 7	i = 8	i = 9	i = 10	i = 11	i = 12	i = 13	i = 14	i = 15
j = 1	+1.000	−0.1547	−0.0360	−0.130	−0.0061	−0.0033	−0.0020	−0.0013	−0.0009	−0.0006	−0.0005	−0.0004	−0.0003	−0.0002	−0.0001
j = 2		+0.5774	−0.1529	−0.0420	−0.0171	−0.0087	−0.0051	−0.0031	−0.0021	−0.0015	−0.0010	−0.0009	−0.0006	−0.0006	−0.0004
j = 3			+0.4472	−0.1382	−0.0408	−0.0178	−0.0093	−0.0057	−0.0037	−0.0026	−0.0018	−0.0013	−0.0010	−0.0007	−0.0007
j = 4				+0.3779	−0.1260	−0.0386	−0.0174	−0.0095	−0.0058	−0.0038	−0.0027	−0.0020	−0.0016	−0.0012	−0.0009
j = 5					+0.3333	−0.1161	−0.0366	−0.0168	−0.0094	−0.0059	−0.0040	−0.0028	−0.0021	−0.0016	−0.0013
j = 6						+0.3015	−0.1081	−0.0346	−0.0163	−0.0091	−0.0058	−0.0041	−0.0028	−0.0022	−0.0016
j = 7							+0.2773	−0.1016	−0.0329	−0.0155	−0.0090	−0.0057	−0.0040	−0.0029	−0.0022
j = 8								+0.2582	−0.0961	−0.0319	−0.0151	−0.0088	−0.0056	−0.0039	−0.0028
j = 9									+0.2425	−0.0913	−0.0301	−0.0146	−0.0085	−0.0055	−0.0039
j = 10										+0.2294	−0.0872	−0.0290	−0.0140	−0.0083	−0.0054
j = 11											+0.2182	−0.0836	−0.0280	−0.0136	−0.0080
j = 12												+0.2085	−0.0270	−0.0132	
j = 13													+0.2000	−0.0776	−0.0261
j = 14														+0.1925	−0.0750
j = 15															+0.1857

Source: Ref 6, 8

puted from these data using Saltykov's method is shown in Table 3. Saltykov's method has been modified by numerous investigators to introduce nonuniform size class intervals, to increase the number of size class intervals beyond 15, and to increase the precision of the estimated three-dimensional size distributions using sophisticated computational algorithms (Ref 85, 93, 94), which are discussed in detail elsewhere (Ref 12).

Size Distribution of Geometrically Similar Nonspherical Particles. DeHoff (Ref 88) has developed a stereological technique for the estimation of the size distribution of ellipsoidal particles from the measurements performed on metallographic plane sections. In this technique, it is assumed that:

- All the particles are either prolate ellipsoids of revolution (for example, cigar-shaped particles), or all of them are oblate ellipsoids of revolution (for example, pancake- shaped particles).
- All the particles have the same axial ratio, and therefore, they are geometrically similar.
- The particles are randomly oriented.

The intersections of the ellipsoidal particles with a metallographic plane yield elliptical particle sections of different sizes and shapes. In the case of oblate ellipsoids of revolution, the major axis of the elliptical particle sections observed in a metallographic plane are measured and the size parameter for the ellipsoids is their major axis. On the other hand, for prolate ellipsoids of revolution, the minor axis of the elliptical sections observed in the metallographic plane are measured, and the ellipsoid size is specified by its minor axis. With this interpretation of the section size and true size parameters, and an introduction of shape factor C, an equation analogous to the one given by Saltykov holds for the ellipsoidal particles (Ref 88):

$$(N_V)_j = C.\sum_{i=j}^{i=K} b(j,\ i).(n_A)_i/\Delta \qquad \text{(Eq 34)}$$

The shape factor C depends on the axial ratio of the ellipsoidal particles, and it can be calculated by using the formula given by DeHoff (Ref 88). As before, $b(j, i$ are Saltykov's coefficients given in Table 1. Analogous procedures are also available for the estimation of the size distribution of cubic (Ref 89) and polyhedral (Ref 90) particles, and lens-shaped grain boundary precipitates (Ref 91).

Multivariate Distributions. Numerous material microstructures contain particle/void/microcrack distributions, where all the features are not geometrically similar and/or are not randomly oriented. In such microstructures, there may also be correlations among the feature sizes, shapes, and their morphological orientations. Bivariate or trivariate distributions are required to characterize such particle/void/microcrack populations. Cruz-Orive (Ref 92) has given a stereological procedure for the estimation of the three-dimensional bivariate size-shape distribution of randomly oriented ellipsoids from the measurements of apparent bivariate size-shape distribution performed in the plane sections, if all the particles can be modeled as either oblate ellipsoids, or prolate ellipsoids (a mixture of prolate and oblate ellipsoids is not permitted). In many material microstructures where the particles/voids can be modeled as ellipsoids (for example, inclusions, creep cavities, etc.), the particles/voids are not randomly oriented (for example, inclusions in a hot-rolled metal, microcracks in particles, creep cavities, etc.), and in such cases, Cruz-Orive's stereological procedure is not useful. The correlations between size and orientation are particularly strong for the features such as microcracks and creep cavities on grain boundaries. For such microstructural features, Gokhale (Ref 38) has given the following stereological equation that relates the three-dimensional bivariate size-orientation distribution of population of features such as microcracks, plate shaped inclusions, and so forth, to the corresponding apparent size-orientation distribution in the vertical metallographic sections:

$$f(r, \alpha) = \frac{4rN_v}{\pi N_A \sin^2\alpha} \cdot \int_r^{r_m}\int_{\pi/2-\alpha}^{\pi/2} \frac{\cos^2\theta \sin\theta g(R,\ \theta)\, d\theta dR}{\left(R^2 - r^2\right)^{1/2}\left(\sin^2\alpha - \cos^2\theta\right)^{1/2}} \qquad \text{(Eq 35)}$$

where $f(r, \alpha)$ is the joint bivariate frequency distribution function in a representative vertical sectioning plane such that $f(r, \alpha)drd\alpha$ is equal to the fraction of the microcrack/plate section traces having the size in the range r to $(r + dr)$ and the orientation in the range α to $(\alpha + d\alpha)$. The function $f(r, \alpha)$ can be estimated from the experimental measurements of r and α on the microcrack traces observed in the vertical planes. The distribution $g(R, \theta)$ is the three-dimensional bivariate microcrack/plate size-orientation distribution function of interest, N_v is the number of microcracks/plates per unit volume in the three-dimensional microstructure, N_A is the average number of microcrack/plate section traces observed per unit area of vertical plane, and r_m is the size of the largest microcrack/plate section trace, which is equal to the true size R_m of the largest microcrack. In practice, $f(r, \alpha)$ is the measured quantity and $g(R, \theta)$ is to be estimated from these data. The numerical procedure for such estimation is described in detail elsewhere (Ref 45). This stereological technique has been recently applied for the estimation of the bivariate size-orientation distribution function of the microcracks observed in the intermetallic inclu-

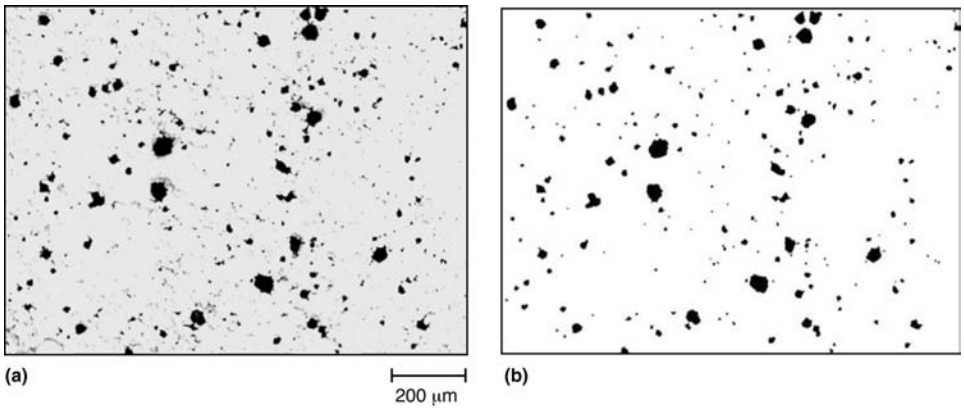

Fig. 28 Use of image processing in estimating size distributions of spherical particles. (a) Unetched microstructure of high-pressure die-cast AM60 Mg-alloy depicting round gas (air) pores and cracklike shrinkage pores. (b) The microstructure in (a) with shrinkage pores removed by using image analysis techniques

Table 2 Two-dimensional section size distribution of gas pores in AM 60 magnesium alloy

See Fig. 28 for microstructure.

Size class (i)	Range of gas pore section diameters [$(i - 1)\Delta$ to $i\Delta$], μm	Number of gas pore sections per mm^2 $(N_A)_i$
1	0–9	39
2	9–18	31
3	18–27	18
4	27–36	7
5	36–45	3
6	45–54	3
7	54–63	1
8	63–72	1

Table 3 Three-dimensional size distribution of the gas pores computed from the section size distribution (Table 2) and Saltykov's coefficients (Table 1) using Saltykov's technique

Size class (j)	Gas pore diameters ($j\Delta$), μm	Number of gas pores in three-dimensions $(N_V)_j$ per mm^3
1	9	3715
2	18	1641
3	27	766
4	36	236
5	45	66
6	54	85
7	63	20
8	72	29

Source: Ref 6, 8

sions in two wrought aluminum alloys loaded in tension and compression (Ref 45); some of these results are shown in Fig. 29. Benes and coworkers (Ref 39) have given a stereological procedure for the estimation of the three-dimensional trivariate size-shape-orientation distribution of ellipsoidal particles/voids from the measurements of the corresponding apparent trivariate particle section size-shape-orientation distribution performed in the vertical sections under the condition that all the particles are either oblate ellipsoids, or they are all prolate ellipsoids.

Spatial Clustering and Correlations

A location is associated with each feature in a microstructure. The statistical distribution of the relative locations of the microstructural features of interest represents their spatial arrangement in a microstructure. Spatial patterns, correlations, clustering, spatial affinity, short- and long-range interactions, pair correlations and higher-order correlations, microstructural gradients, segregations, and so forth, are important facets of the spatial arrangement of microstructural features. It is well known that these attributes of microstructural geometry affect numerous mechanical and physical properties of materials. Although theoretical statistics literature contains numerous quantitative descriptors that reflect various aspects of the spatial arrangement of ensembles of features in two- and three-dimensional space (Ref 1), flexible and general experimental techniques for estimation of such descriptors in the opaque material microstructures are still under development. Nevertheless, during the past decade or so, considerable progress has been made in the development of practical stereological techniques for the estimation of some important descriptors of spatial arrangement such as two-point correlation function (Ref 37), radial distribution function (Ref 22, 23, 36), nearest-neighbor distributions (Ref 22, 23, 36, 95), and coordination number distribution (Ref 35, 95). These recent developments are briefly described in the paragraphs that follow.

Two-Point Correlation Function. In a 3-D microstructure containing two phases, for example, particles (phase 1) and matrix (phase 2), the two-point correlation function $P_{11}(r, \theta, \phi)$ is the probability that both the end-points of a randomly located straight line of length r and angular orientation (θ, ϕ) are contained in phase 1 (i.e., particles). One can similarly define $P_{22}(r, \theta, \phi)$, where both the end points are in phase 2 (matrix), and $P_{12}(r, \theta, \phi)$, where one end of the line is in phase 1 and the other is in phase 2. Although for a two-phase microstructure there are four possible two-point correlation functions, only one of the four is independent. Therefore, in this contribution, only the two-point function $P_{11}(r, \theta, \phi)$ is considered. If the microstructure has a symmetry axis, then it is most efficient to choose the symmetry axis as the Z-axis of the reference frame (vertical axis). In such a case, $P_{11}(r, \theta, \phi)$ does not depend on ϕ, and consequently, $P_{11}(r, \theta)$ measured in any one vertical plane (having symmetry axis as vertical axis) completely specifies the direction dependence of the two-point correlation function.

To capture the short-range as well as long-range spatial patterns, in a majority of material microstructures the two-point correlation data are required over the distances ranging from 1 to 500 μm at a resolution of about 0.5 μm. Therefore, the two-point correlation function cannot be measured from the usual "single field of view" microstructural images because such images either lack resolution (when magnification is low) or they lack the long-range spatial information (when magnification is high). Consequently, for the experimental measurement of the two-point correlation function, it is essential to create a seamless "montage" of very large number of contiguous microstructural fields of view (~100 fields), as explained in section "Large-Area Disector (LAD) for Efficient and Unbiased Estimation of Number Density" (see Fig. 21). As a montage can be at a high resolution (typically 0.5 μm resolution) and of very large area (typically few mm^2 or so), it can capture both short- and long-range spatial patterns and correlations.

A computer code has been recently developed for the calculation of the two-point correlation function from the input image of a binary microstructural montage (Ref 37). The program reads the binary image and asks the user for the input to the maximum length (l_m) to which the two-point function is to be measured. A virtual rectangle inside the binary image, known as measurement frame, is then created such that each point inside this frame is at least l_m distance from the nearest edge. The computation begins with the reading of the gray value of the first pixel (base point) in the measurement frame to identify whether the point belongs to phase 1 (black) or phase 2 (white). The next step consists of reading of gray value of all the pixels inside a circle of radius l_m drawn around the base point, and computation of their Cartesian distance r from the base point and angle θ with the vertical axis. The program separately stores all the length segments whose both end pixels are black. This process is repeated for all the base points inside the measurement frame. Once the occurrences of all the required distances and angles are recorded, the probability is computed by dividing the number segments of given length and orientation whose both end pixels are black by the total number of the segments having the same length and orientation. The process is then repeated for different distances and orientation angles to generate detailed data on the direction-dependent two-point correlation function $P_{11}(r,$

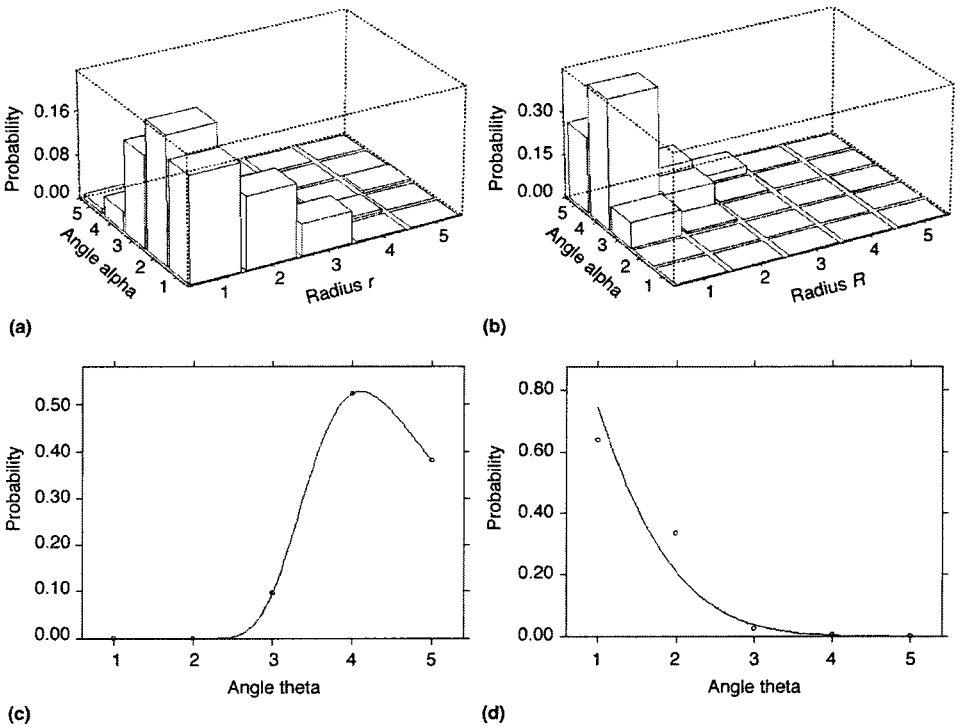

Fig. 29 Estimation of the bivariate size-orientation distribution function of microcracks. (a) Bivariate size-orientation distribution of the microcrack traces in a vertical metallographic plane where the vertical axis is the loading direction, in the 6061 aluminum alloy under a uniaxial compressive stress deformed to 0.7 strain. (b) The estimated 3-D bivariate size and orientation distribution of the microcracks. All angles are measured with respect to the loading direction (vertical axis). In compression, the majority of the microcracks are parallel to the direction of applied compressive load. (c) Marginal 3-D orientation distribution of the microcracks under uniaxial compression at 0.7 strain. (d) Marginal 3-D orientation distribution of the microcracks under uniaxial tension. Observe that majority of the microcracks are now perpendicular to the loading direction. For all the distributions, the size class interval for radius is 0.69 μm, and for the orientation angle, it is 18°. Source: Ref 45

θ). Since a montage is a large image, calculation of the two-point function over the distances from 1 to 500 μm typically involves measurements on about 7 million base pixels, and 4 million top pixels for each base pixel. This amounts to about 28×10^{12} measurements, with the distance and angle computed for each such measurement.

This technique has been recently applied to quantify spatial clustering in the microstructures of an extruded metal matrix composite containing SiC particles in an aluminum alloy matrix (Ref 37). Figures 30(a) and (b) show two of the microstructures that have exactly the same volume fraction and size distribution of SiC particle: the only difference in these two microstructures is the spatial clustering of the SiC particles. Figure 30(c) depicts the normalized two-point correlation function in these microstructures along the extrusion direction (chosen vertical axis), and Fig. 30(d) depicts the normalized two-point correlation for the transverse direction. Observe that these correlation functions nicely capture the differences in the clustering tendencies and long-range spatial patterns in the two microstructures in Fig. 30(a) and (b), which demonstrates the utility of two-point correlation functions for mathematical representation of the clustering and spatial heterogeneity in microstructures (Ref 37).

Coordination Number Distribution. In the microstructures containing contiguous grains/particles, coordination number is an important geometric parameter. The coordination number of a grain/particle is the number of other grains/particles in direct contact with it. In general, a distribution of coordination numbers exists, which is an important descriptor of the short-range spatial arrangement of grains/particles. The mean coordination number (often referred to as just coordination number or connectivity in the sintering literature) is the average value of the coordination number distribution in the three-dimensional microstructure. The mean coordination number affects the mechanical response of liquid phase sintered materials (Ref 96), and it appears as a parameter in the theories of densification (Ref 97). There is often a correlation between the size of a grain and its coordination number. Therefore, a bivariate distribution of the 3-D coordination numbers that expresses the fraction of the grains having a given coordination number and having size in a certain narrow range is of importance. The mean coordination number and its distribution cannot be estimated from any measurements performed on independent 2-D metallographic sections. Direct observations on the 3-D microstructure are required for the estimation of the coordination number distribution. Further, to minimize the edge effects, the measurements must be performed on a large volume of the 3-D microstructure observed at a high resolution. Recently, a montage serial sectioning technique has been developed for creation of such a large volume of 3-D microstructure of an opaque material at a high resolution (~1 μm). The method combines the montage technique for creation of a large contiguous area of a metallographic plane at a high resolution with the serial sectioning method and 3-D digital image processing (see Fig. 31). The montage serial sections are stacked together and aligned (Fig. 31b and c), and the 3-D microstructure is reconstructed using 3-D image analysis software (Ref 32–35, 95). Figure 32 depicts small segments of two surface-rendered 3-D microstructures reconstructed in this manner, where the matrix was removed using image processing. To determine the coordination number of a grain/particle, it is then necessary to examine its local microstructural environment and count the number of other grains/particles in contact with it. These observations are repeated over a large

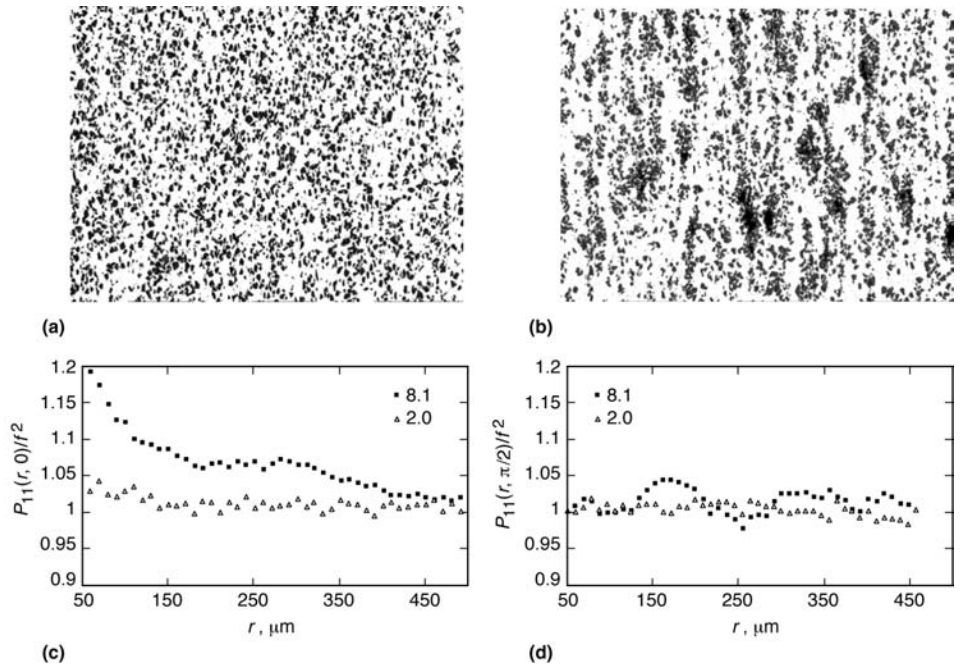

Fig. 30 Two-point correlation function. (a) Microstructure of a metal-matrix composite having uniform random distribution of SiC particles in an aluminum alloy matrix. The data points in (c) and (d) for this specimen are the open triangles. (b) Metal-matrix composite having highly clustered distribution of SiC particles in the particle-rich bands parallel to the extrusion direction (*Y*-axis of the micrograph). This specimen has exactly the same volume fraction and size distribution of the SiC particles as that in (a). The data points in (c) and (d) for this specimen are the dark rectangles. (c) Normalized two-point correlation function $P_{11}(r, 0)$ along the direction parallel to the extrusion direction (*Y*-axis). The dark rectangle data points for the composite having clustered SiC particles—i.e., (b)—do not reach the saturation value even at distances of 450 μm. (d) The normalized two-point correlation function $P_{11}(r, \pi/2)$ along the transverse direction. The data corresponding to the specimen with clustered SiC particles—i.e., (b)—show long-range oscillations that correspond to particle-rich and particle-poor regions. Source: Ref 37

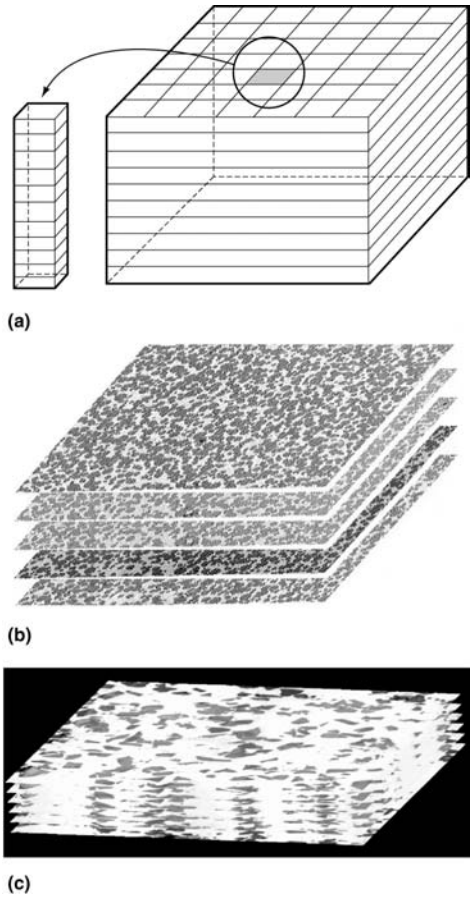

Fig. 31 Montage serial sectioning. The process involves creation of montages of large number of serial sections grabbed at a high resolution and then (a) aligned and stacked together to reconstruct a 3-D microstructure. (b) A stack of five montage serial sections of microstructure of a liquid phase sintered W-Ni-Fe alloy showing tungsten grains. The montages have been digitally compressed for presentation. Source: Ref 95. (c) A stack of aligned five serial sections of microstructure of metal-matrix composite showing SiC particles in aluminum alloy matrix. Each serial section shown here is a very small segment of the actual montages created. Source: Ref 98

number of grains/particles sampled in an unbiased manner, and the coordination number distribution is computed from such data. Figure 33 shows one such three-dimensional bivariate coordination number distribution of tungsten grains in a W-Ni-Fe alloy that was liquid phase sintered in the microgravity environment of the NASA's space shuttle Columbia. Table 4 shows the data on the mean coordination number of the tungsten grains in this alloy processed in the microgravity and normal gravity environments. Observe that the microgravity environment leads to the microstructure that is more open and therefore has a lower mean coordination number.

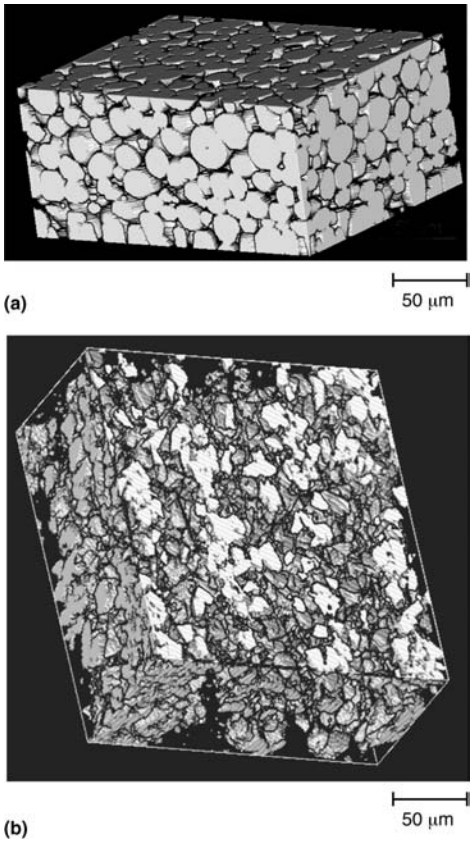

Fig. 32 Surface-rendered images of small volume segments from large-volume high-resolution 3-D microstructures reconstructed from large number (~100) of montage serial sections. (a) 3-D image depicting tungsten grains in a liquid phase sintered W-Ni-Fe-alloy. Source: Ref 35, 95. (b) SiC particles clustered in the bands in the microstructure of a metal-matrix composite. Source: Ref 98

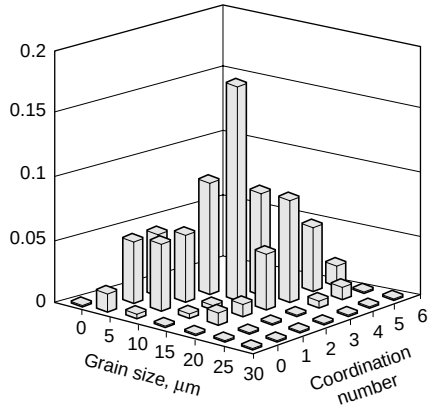

Fig. 33 Bivariate distribution of three-dimensional coordination numbers of tungsten grains in a 83 wt% W-Ni-Fe alloy specimen liquid phase sintered in microgravity environment for 1 min at 1507 °C (2745 °F). The *Z*-axis is the fraction of grains having a given coordination number, and grain size in a given range. Source: Ref 35, 95

Nearest-Neighbor Distribution Functions. The spatial arrangement of particle/grain centers in the 3-D microstructure can also be characterized in terms of a series of nearest-neighbor distribution functions. The first nearest-neighbor distribution function is given by the probability density function $\psi_1(r)$, such that $\psi_1(r)dr$ is the probability that there is no other particle/grain center in a sphere of radius r around a typical particle/grain, and there is at least one particle/grain center in the spherical shell of radii r and $(r + dr)$. The second nearest-neighbor distribution function is characterized by the probability density function $\psi_2(r)$ such that $\psi_2(r)dr$ is the probability that there is exactly one other particle/grain center in a sphere of radius r around a typical particle/grain, and there is at least one particle/grain center in the spherical shell of radii r and $(r + dr)$. In general, nth nearest-neighbor distribution function $\psi_n(r)$ is the probability density function such that $\psi_n(r)dr$ is the probability

Table 4 Mean three-dimensional coordination number of tungsten grains in 83 wt% W-Ni-Fe alloy liquid phase sintered at 1507 °C (2745 °F)

Normal gravity		Microgravity	
1 min	120 min	1 min	120 min
3.7	4.3	2.9	2.9

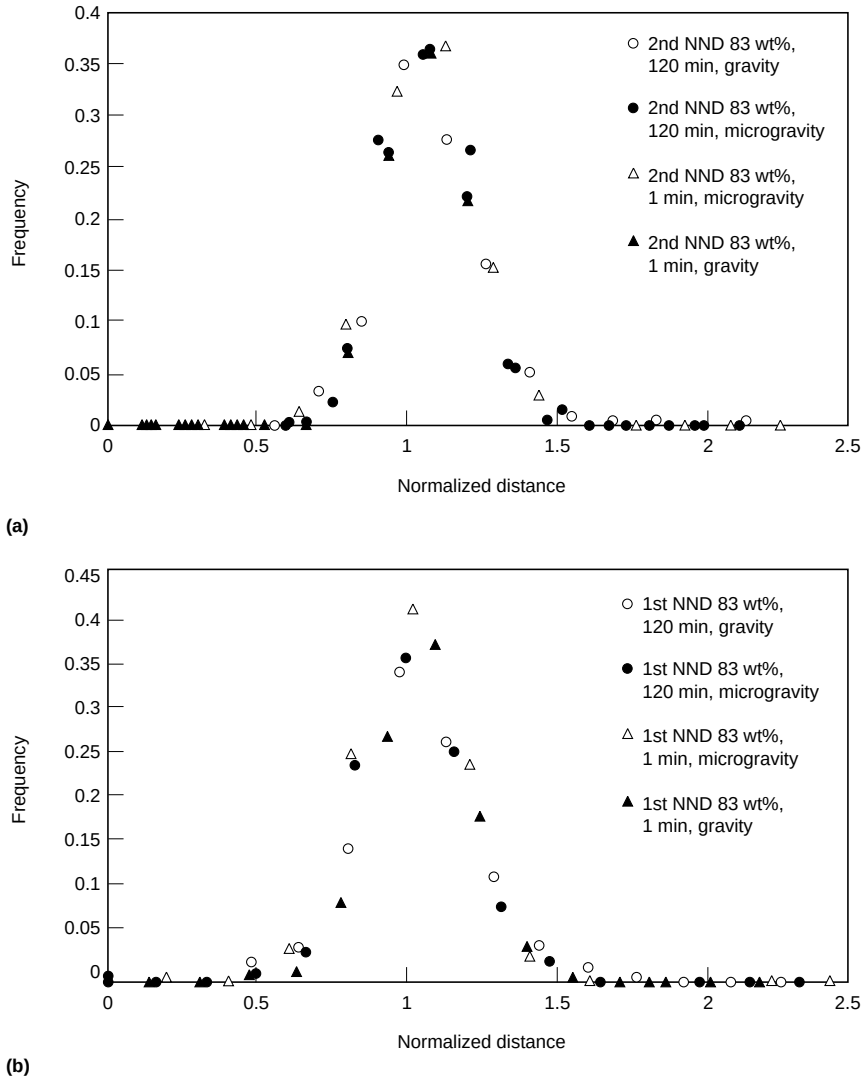

Fig. 34 Normalized 3-D nearest-neighbor distributions of tungsten grain centers in the specimens of W-Ni-Fe alloys under different processing conditions. (a) First nearest-neighbor distribution. (b) Second nearest-neighbor distribution. Source: Ref 95

that there are exactly $(n - 1)$ other particle centers in a sphere of radius r around a typical particle, and there is at least one particle center in the spherical shell of radii r and $(r + dr)$. The first nearest-neighbor distribution describes the short-range spatial arrangement of the particle/grain centers; progressively higher-order nearest-neighbor distributions characterize the spatial arrangement of the particles at the larger distances.

The nearest-neighbor distributions and the corresponding mean nearest-neighbor distances in the 3-D microstructure cannot be estimated from any measurements performed on independent 2-D metallographic sections, or by using a disector. Direct measurements on the 3-D microstructure are required for the estimation of these statistical distributions. Further, to minimize the edge effects, the measurements must be performed on a large volume of 3-D microstructures observed at a high resolution, which is possible via the montage serial sectioning technique (Fig. 33) explained in the previously. The coordinates of the centroids of the particles/grains can be measured in the reconstructed 3-D images; the nearest-neighbor distributions can be then computed from such data in a straightforward manner. Figure 34 shows normalized first and second nearest-neighbor distribution of the centers of the tungsten grains in the liquid phase sintered microstructures of a W-Ni-Fe alloy processed in the normal gravity and microgravity (Ref 95). In these plots, the nearest-neighbor distances are normalized by the average grain diameters. Observe that the normalized nearest-neighbor distributions are almost time invariant, indicating that the grain-coarsening process only leads to a scale change in the short-range spatial arrangement of the tungsten grains in these microstructures.

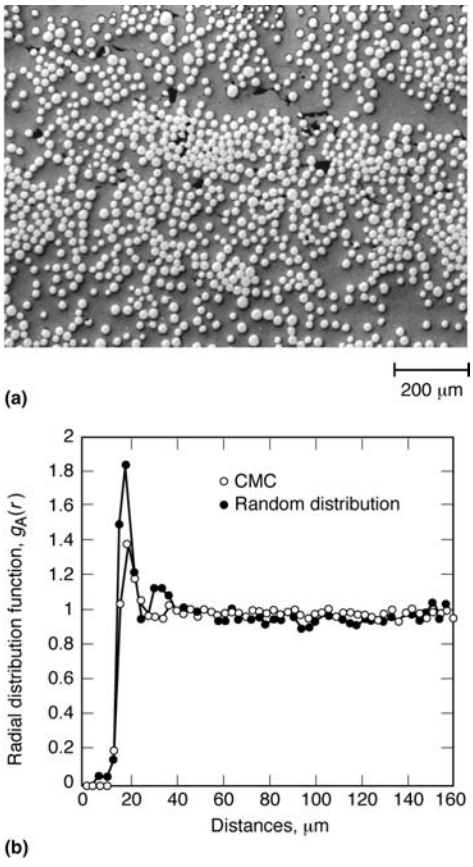

Fig. 35 Radial distribution function. (a) Microstructure of a ceramic-matrix composite containing aligned continuous fibers of SiC (nicalon) having a nonuniform spatial distribution, consisting of fiber-rich and fiber-poor regions, observed in the transverse section. (b) Radial distribution function $g_A(r)$ of the fiber centers in the composite (dark circles) and the corresponding radial distribution function in a computer-simulated composite having the same volume fraction and size distribution of the fibers, but a uniform random spatial distribution (open circles). Source: Ref 36

Radial distribution function is another important descriptor of the short-range, intermediate-range, long-range spatial arrangement of particle/grains centroids in a microstructure. The radial distribution function $g(R)$ is equal to the ratio of the number of particle centers in a spherical shell of radii R and $(R + dR)$ around a typical particle and $(4\pi R^2 N_V dR)$, where N_V is the number density of the particles. For any microstructure, as $R \rightarrow \alpha$, $g(R) \rightarrow 1$. The radial distribution function of the particle/grain section centers in a 2-D metallographic plane or in a 2-D microstructure can be defined in an analogous manner. The 3-D radial distribution function cannot be estimated from any measurements performed on independent 2-D metallographic sections, or by using a disector. Practical stereological techniques for the estimation of 3-D radial distribution function have not been yet developed. However, the 2-D radial distribution function of the particle/fiber sections can be estimated efficiently in an unbiased manner (free of edge effects) using large area high-resolution montages as described elsewhere (Ref 22). In the materials such as composites containing continuous aligned fibers, the radial distribution function of the fiber centers in the transverse section essentially contains all the 3-D information on the spatial arrangement of fibers. In such microstructures, the 2-D radial distribution function in the transverse section is useful for characterization of the spatial arrangement of fibers. Figure 35(a) shows microstructure of such a composite containing aligned continuous SiC (nicalon) fibers in a glass ceramic (MAS) matrix observed in the transverse section. Observe that the spatial distribution of the fibers is not uniformly random, because there are fiber-rich and fiber-poor bands in the microstructure. Figure 35(b) shows the experimentally measured radial distribution function of the centers of the fibers in this microstructure (Ref 23). The radial distribution function of a uniform random microstructure having the same fiber volume fraction and size distribution obtained via computer simulations is superimposed on the experimental data. Observe that the first peak in the simulated data is much lower than that in the experimental data indicating short clustering of the fibers in the composite. Further, at the distances larger than 40 μm, the experimental data consistently remain slightly below 1.0 indicating presence of fiber-poor regions in the microstructure. These experimental data have been used to develop a computer-simulated nonuniform microstructure that has the nonuniform spatial arrangement that is statistically similar to that in the composite. Such microstructure models can be used to predict the effects of microstructural variations on the mechanical response of the composite using the finite elements (FE) based or other computational mechanics techniques (Ref 99).

ACKNOWLEDGMENT

The Division of Materials Research of the U.S. National Science Foundation (NSF) and the Metallic Materials Program of the Air Force Office of Scientific Research (AFOSR) supported this work through the research grants DMR-9816618 and F49620-01-1-0045, respectively. Joseph Akkara and Bruce MacDonald are the Program Managers for the NSF grant, and C.S. Hartley is the Program Manager for the AFOSR grant. Additional financial support was provided by American Foundry Society (AFS)/United States Consortium for Automotive Research (USCAR) Project through the Structural Cast Magnesium Development (SCMD) program for which Richard Osborne, Donald Penrod, and Joseph Santner are the Program Managers. The financial support from the funding agencies is gratefully acknowledged. Published/unpublished research results of numerous past and present students of the author have been used in this contribution. The author gratefully acknowledges the contributions of his students K. Bodlak, A. Cottet, N.U. Deshpande, M.D. Dighe, W.J. Drury, M. Hlawiczkova, T. Joenes, Z. Shan, A. Tewari, S. Yang, H. Agarwal, A. Balasundaram, Felipe Correa, Soon Gi Lee, Scott Lieberman, Pascal Louis, Yuxiong Mao, T. H. Mirabelli, B.R. Morris, S. Mukherjee, G. R. Patel, H. Singh, and W.T. Whited.

REFERENCES

1. D. Stoyan, S. Kendall, and J. Mecke, *Stochastic Geometry and Its Applications*, 2nd ed., John Wiley and Sons, 1995
2. L.A. Santalo, *Integral Geometry and Geometric Probability*, Addison-Wesley, 1976
3. A. Gray, *Modern Differential Geometry of Curves and Surfaces*, 2nd ed., CRC Press, London, 1997
4. P.R. Mouton, *Principles and Practices of Unbiased Stereology: An Introduction for Bioscientists*, The Johns Hopkins University Press, 2002
5. F. Chayes, *Petrographic Modal Analysis*, John Wiley, 1956
6. E.E. Underwood, *Quantitative Stereology*, Addison Wesley, 1970
7. R.T. DeHoff and F.N. Rhines, *Quantitative Microscopy*, McGraw Hill, 1968
8. S.A. Saltykov, *Stereometric Metallography*, 2nd ed., Metallurgizdat, Moscow, 1958

9. A.J. Baddeley, H.J.G. Gundersen, and L.M. Cruz Orive, Estimation of Surface Area Using Vertical Sections, *J. Microsc.*, Vol 142, 1986, p 259–276
10. A.M. Gokhale and W.J. Drury, Efficient Estimation of Microstructural Surface Area Using Trisector, *Metall. Trans. A*, Vol 25A, 1994, p 919–928
11. B.R. Morris, A.M. Gokhale, and G.F. Vander Voort, Estimation of Grain Size in Anisotropic Materials, *Metall. Mater. Trans. A*, Vol 29A, 1998, p 237–244
12. J. Ohser and F. Muecklich, *Statistical Analysis of Microstructures in Material Science*, John Wiley & Sons, 2000
13. A.M. Gokhale, Unbiased Estimation of Curve Length in 3D Using Vertical Slices, *J. Microsc.*, Vol 159, 1990, p 133–141
14. A.M. Gokhale, Estimation of Length Density L_v from Vertical Slices of Unknown Thickness, *J. Microsc.*, Vol 167, pt. I, 1992, p 1–8
15. A.M. Gokhale, Utility of Horizontal Slice for Stereological Characterization of Lineal Features, *J. Microsc.*, Vol 170, pt. 1, 1993, p 3–8
16. L.M. Cruz Orive and X. Gual-Arnau, Precision of Circular Systematic Sampling, *J. Microsc.*, Vol 207, 2002, p 225–242
17. A.M. Gokhale and N.U. Deshpande, Stereology of Anisotropic Microstructures, *Quantitative Microscopy and Image Analysis*, D.J. Diaz, Ed., ASM International, 1994, p 73–82
18. P.R. Mouton, A.M. Gokhale, N.L. Ward, and M.J. West, Unbiased Length Estimation Using Isotropic Spherical Probes, *J. Microsc.*, Vol 206, 2002, p 54–64
19. D.C. Sterio, The Unbiased Estimation of Number and Size of Arbitrary Particles Using Disector, *J. Microsc.*, Vol 134, 1984, p 127–136
20. A.M. Gokhale and A. Tewari, Efficient Estimation of Number Density in Opaque Material Microstructures Using Large Area Disector (LAD), *J. Microsc.*, Vol 200, pt. 3, 2000, p 277–283
21. J.P. Kroustrup and H.J.G. Gundersen, Estimating the Number of Complex Particles Using the ConnEulor Principle, *J. Microsc.*, Vol 203, 2001, p 314–320
22. L. Pascal and A.M. Gokhale, Application of Image Analysis for Characterization of Spatial Arrangement of Features in Microstructures, *Metall. Mater. Trans.*, Vol 26A, 1995, p 1449–1456
23. S. Yang, A. Tewari, and A.M. Gokhale, Modeling of Non-Uniform Spatial Arrangement of Fibers in a Ceramic Matrix Composite, *Acta Mater.*, Vol 45, 1997, p 3059–3069
24. C. Babu Rao, P. Kalyansundaram, K.K. Ray, and B. Raj, *Image Analysis in Materials and Life Sciences*, Oxford and IBH, New Delhi, India, 2000
25. J. Serra, *Image Analysis and Mathematical Morphology*, Academic Press, 1982
26. J.C. Russ, *The Image Processing Handbook*, CRC Press, London, 2001
27. P. Velecky and J. Pospisil, Digital Image Processing for Evaluation of the Internal Microstructure Characteristics of Cemented Carbides, *Optik*, Vol 111, 2000, p 493–496
28. A. Balasundaram and A.M. Gokhale, Quantitative Characterization of Spatial Arrangement of Shrinkage and Gas (Air) Pores in Cast Magnesium Alloys, *Mater. Charact.*, Vol 46, 2001, p 419–426
29. A.J. Schwartz, M. Kumar, and B.L. Adams, *Electron Backscatter Diffraction in Materials Science*, Plenum Press, 2000
30. F.J. Humphreys, Quantitative Metallography by Electron Backscattered Diffraction, *J. Microsc.*, Vol 195, 1999, p 170–185
31. J.K. Stevens, L.R. Mills, and J.E. Trogadis, *Three-Dimensional Confocal Microscopy*, Academic Press, London, UK, 1994
32. A. Tewari and A.M. Gokhale, Application of Serial Sectioning for Estimation of 3D Grain Size Distribution in a Liquid Phase Sintered Microstructure, *Mater. Charact.*, Vol 46, 2001, p 329–335
33. A. Tewari, M.D. Dighe, and A.M. Gokhale, Application of Digital Image Processing for Reconstruction of Three-Dimensional Microstructure From Serial Sections, *Mater. Charact.*, Vol 44, 2000, p 259–269
34. M.V. Kral, and G. Spanos, 3D Analysis of Cementite Precipitates, *Acta Mater.*, Vol 47, 1999, p 711–724
35. A. Tewari, A.M. Gokhale, and R.M. German, Effect of Gravity on Three-Dimensional Coordination Number Distribution in Liquid Phase Sintered Microstructures, *Acta Mater.*, Vol 47, 1999, p 3721–3734
36. S. Yang, A. Tewari, and A.M. Gokhale, An Experimental Method for Quantitative Characterization of Spatial Distribution of Fibers in Composites, *Developments in Materials Characterization Technologies*, G.F. Vander Voort and J.J. Frial, Ed., ASM International, 1996 p 33–43
37. A. Tewari, A.M. Gokhale, J.E. Spowart, and D.B. Miracle, Quantitative Characterization of Spatial Clustering in Three-Dimensional Microstructures Using Two-Point Correlation Functions, *Acta Mater.*, Vol 52, 2004, p 307–319
38. A.M. Gokhale, Estimation of Bivariate Size and Orientation Distribution of Microcracks, *Acta Metall.*, Vol 44, 1996, p 475–485
39. V. Benes, V. Jiruses, and M. Slamova, Estimation of Trivariate Size-Shape-Orientation Distributions from Vertical Sections, *Acta Mater.*, Vol 45, 1997, p 1105–1110
40. L. Hengcheng, Y. Sun, and S. Guoxiong, Correlation between Mechanical Properties and Amount of Dendritic Alpha-Al Phase in As-Cast Near-Eutectic Al-11.6% Si Alloys Modified with Strontium, *Mater. Sci. Eng. A*, Vol 335, 2002, p 62–66
41. M. Sozanska, A. Maciejny, C. Dagbert, J. Galland, and L. Hyspecka, Use Of Quantitative Metallography in the Evaluation of Hydrogen Action During Martensitic Transformations, *Mater. Sci. Eng. A*, Vol A273, 1999, p 485–490
42. Q. Meng, Y. Rong, S. Chen, and T.Y. Hsu, The Relationship of the Volume Fraction of Martensite vs. Plastic Strain in a Fe-Mn-Si-Cr-N Shape Memory Alloy, *Mater. Lett.*, Vol 50, 2001, p 328–332
43. H. Agarwal, A.M. Gokhale, S. Graham, and M.F. Horstemeyer, Quantitative Characterization of Three-Dimensional Damage Evolution in a Wrought Al-Alloy under Tension and Compression, *Metall. Mater. Trans.*, Vol 33A, 2002, p 2599–2606
44. M.P. Black, R.L. Higginson, and C.M. Sellars, Effect of Strain Path on Recrystallization Kinetics During Hot Rolling of Al-Mn, *Mater. Sci. Technol.*, Vol 17, 2001, p 1055–1060
45. K. Bodlak, A. Balasundaram, A.M. Gokhale, and V. Benes, Unfolding of Three-Dimensional Bivariate Size-Orientation Distribution of Microcracks, *Acta Mater.*, Vol 51, 2003, p 3131–3143
46. R.A. Vandermeer, N. Hansen, X. Huang, J. Jensen, E.M. Laurdisen, T. Leffers, W. Pantleon, T.J. Sabine, and J.A. Wert, Kinetic Aspects of Nucleation and Growth in Recrystallization, *Proc. 21st Riso International Symposium on Materials Science* (Roskilde, Denmark), 2000, p 179–200
47. J.A. Griggs, K.J. Anusavice, and J.J. Mecholsky, Jr., Devitrification and Microstructural Coarsening of a Fluoride-Containing Barium Aluminosilicate Glass, *J. Mater. Sci.*, Vol 37, 2002, p 2017–2022
48. K.-W. Moon, W.J. Boettinger, U.R. Kattner, C.A. Handwerker, and D.-J. Lee, The Effect of Pb Contamination on the Solidification Behavior of Sn-Bi Solders, *J. Electron. Mater.*, Vol 30, 2001, p 45–52
49. F.G. Caballero, C. Garcia de Andres, and C. Capdevila, Characterization and Morphologic Analysis of Pearlite in a Eutectoid Steel, *Mater. Charact.*, Vol 45, 2000, p 111–116
50. K.J. and H. Conrad, Microstructure Coarsening During Static Annealing of 60Sn40Pb Solder Joints. I. Stereology, *J. Electron. Mater.*, Vol 30, 2001, p 1294–1302
51. S. Spangel, E. Matthaei-Schulz, A. Schulz, H. Vetters, and P. Mayr, Influence of Carbon and Chromium Content and Preform Shape on the Microstructure of Spray Formed Steel Deposits, *Mater. Sci. Eng. A*, Vol A326, 2002, p 26–39
52. J. Wosik, H.J. Penkalla, K. Szot, B. Dubiel, and F.C. Schubert, The Influence of Various Microscopic Techniques on the Quantification of Stereological Structure Parameters in Waspaloy Alloy, *Prakt. Metallogr.*, Vol 39, 2002, p 140–154
53. W. Yunxin, R.M. German, D. Blaine, B. Marx, and C. Schlaefer, Effects of Residual Carbon Content on Sintering Shrinkage, Microstructure and Mechanical Properties of

Injection Molded 17-4 PH Stainless Steel, *J. Mater. Sci.*, Vol 37, 2002, p 3573–3583
54. M. Grange, J. Besson, and E. Andrieu, An Anisotropic Gurson Type Model to Represent the Ductile Rupture of Hydrided Zircaloy-4 Sheets, *Int. J. Fract.*, Vol 105, 2000, p 273–293
55. N.U. Deshpande, A.M. Gokhale, D.K. Denzer, and J. Liu, Relationship between Fracture Toughness, Fracture Path, and Microstructure of 7050 Aluminum Alloy—I: Quantitative Characterization, *Metall. Mater. Trans. A*, Vol 29A, 1998, p 1191–1201
56. H. Agarwal, A.M. Gokhale, S. Graham, and M.F. Horstemeyer, Anisotropy of Intermetallic Particle Cracking Damage Evolution in an Al-Si-Mg Base Wrought Aluminum Alloy under Uniaxial Compression, *Metall. Mater. Trans. A*, Vol 33A, 2002, p 3443–3448
57. H. Agarwal, A.M. Gokhale, and S. Graham, Void Growth in 6061 Al-Alloy under Triaxial Stress State, *Mater. Sci. Eng.*, Vol 341 (No. 1–2), 2003, p 35–42
58. A.K. Balasundaram, A.M. Gokhale, S. Graham, and M.F. Horstemeyer, Three Dimensional Particle Cracking Damage Development in an Al-Mg Base Alloy, *Mater. Sci. Eng.*, Vol 355 (No. 1–2), 2003, p 368–383
59. Z. Zhang and F. Wang, Research on the Deformation Strengthening Mechanism of a Tungsten Heavy Alloy by Hydrostatic Extrusion, *Int. J. Refract. Met. Hard Mater.*, Vol 19, 2001, p 177–182
60. Y. Wu, R.M. German, D. Blaine, B. Marx, and C. Schlaefer, Effects of Residual Carbon Content on Sintering Shrinkage, Microstructure and Mechanical Properties of Injection Molded 17-4 PH Stainless Steel, *J. Mater. Sci.*, Vol 37, 2002, p 3573–3583
61. C.S. Smith and L. Guttman, Measurement of Internal Boundaries in Three-Dimensional Structures by Random Sectioning, *Trans. AIME*, Vol 97, 1953, p 81
62. A.M. Gokhale and W.T. Whited, Measurements of Growth Rates of Thermally Induced Micro-cracks in a Metal Matrix Composite, *Developments in Ceramics and Metal Matrix Composites*, K. Upadhya, Ed., TMS, 1992, p 273–286
63. A.M. Gokhale, W.J. Drury, and W.T. Whited, Quantitative Microstructural Analysis of Anisotropic Materials, *Mater. Charact.*, Vol 31, 1993, p 11–18
64. L. Karlsson and A.M. Gokhale, Stereological Estimation of Mean Linear Intercept Length in Metallography Using Vertical Sections and Trisector, *J. Microsc.*, Vol 186, 1997, p 143–152
65. E.A. Stocks, J.M. McArthur, J.W. Griffin, and P.R. Mouton, An Unbiased Method for Estimation of Total Epidermal Nerve Fiber Length, *J. Neurocyt.*, Vol 25, 1996, p 11–18
66. P.J. McMillan, J.O. Archambeau, and A.M. Gokhale, Morphometric and Stereological Analysis of Cerebral Cortical Microvessels Using Optical Sections and Thin Slices, *Acta Stereol.*, Vol 13, 1994, p 33–38
67. S. Batra, M.F. Konig, and L.M. Cruz Orive, Unbiased Estimation of Capillary Length from Vertical Slices, *J. Microsc.*, Vol 178, 1994, p 152–159
68. C.V. Howard, L.M. Cruz Orive, and H. Yaegashi, Estimating Neuron Dendritic Length in 3D From Total Vertical Projections and Vertical Slices, *Acta Neurol. Scand., Suppl.*, Vol 137, 1992, p 14–19
69. M. Hlawiczkova, A.M. Gokhale, and V. Benes, Efficiency and Bias of Length Density Estimator, *J. Microsc.*, Vol 204, 2001, p 2226–2231
70. J.E. Hilliard and J.W. Cahn, An Evaluation of Procedures in Quantitative Metallography for Volume Fraction Analysis, *Trans. AIME*, Vol 221, 1961, p 344–354
71. H.J.G. Gundersen and E.B. Jensen, The Efficiency of Systematic Sampling in Stereology and Its Prediction, *J. Microsc.*, Vol 121, 1987, p 65–73
72. L.M. Cruz Orive, Systematic Sampling in Stereology, *Bull. Int. Stat. Inst.*, Vol 55, 1993, p 451–468
73. L.M. Cruz Orive, On the Precision of Systematic Sampling: A Review of Matheron's Transitive Methods, *J. Microsc.*, Vol 153, 1985, p 518–530
74. H.J.G Gundersen, E.B. Kiru, and J. Neilsen, The Efficiency of Systematic Sampling in Stereology, *J. Microsc.*, Vol 193, 1999, p 199–211
75. E. Kreyszig, *Advanced Engineering Mathematics*, 6th ed., John Wiley & Sons, 1988
76. H.J.G. Gundersen, Note on Estimation of Number Density of Arbitrary Profiles: The Edge Effect, *J. Microsc.*, Vol 11, 1977, p 219–223
77. G.F. Vander Voort, Examination of Some Grain Size Measurement Problems, *Metallography: Past, Present, and Future*, G.F. Vander Voort, F.J. Warmuth, S.M. Purdy, and A. Szirmae, Ed., STP 1165, ASTM, 1993, p 266–294
78. G.F. Vander Voort, *Metallography: Principles and Practice*, ASM International, 1999
79. A.M. Gokhale, Estimation of Average Size of Convex Particle, *Metall. Trans. A*, Vol 17A, 1986, p 742–745
80. J. Gurland, Measurement of Grain Contiguity in Two-Phase Alloys, *Trans. AIME*, Vol 212, 1958, p 452–456
81. R.L. Fullman, Measurement of Particle Sizes in Opaque Bodies, *Trans. AIME*, Vol 197, 1953, p 47
82. H.W. Chalkley, J. Cornfield, and H. Park, A Method for Estimating Volume-Surface Ratio, *Science*, Vol 110, 1949, p 295
83. "Standard Test Methods for Determining Average Grain Size," E 112, *Annual Book of ASTM Standards*, ASTM
84. A.M. Gokhale, Interpretation of Grain Size Descriptors, *Trans. Ind. Inst. Metals*, Vol 35, 1982, p 595–600
85. W.M. Visscher and A.S. Goldman, Estimating the Distribution of Spherical Particles from Plane Sections: An Optimal Algorithm for Solution of the Abel Integral Equation, *Siam. J. Sci. Stat. Comput.*, Vol 4, 1983, p 280–290
86. G.M. Tallis, Estimating the Distribution of Spherical and Elliptical Bodies from Plane Sections, *Biometrics*, Vol 26, 1970, p 87–90
87. P. Luchini, A. Pozzi, and C. Ronchi, Evaluation of Statistical Distribution of Spherical Objects from Measurements of Metallographic Cross-Sections, *Meccanica*, Vol 19, 1984, p 127–133
88. R.T. DeHoff, The Determination of Size Distribution of Ellipsoidal Particles from Measurements Made on Random Plane Sections, *Trans. Metall. Soc. AIME*, Vol 224, 1962, p 474–477
89. J. Osher and M. Nippe, Stereology of Cubic Particles: Various Estimators for the Size Distribution, *J. Microsc.*, Vol 187, 1997, p 22–30
90. J. Osher and F. Mucklich, Stereology of Some Classes of Polyhedrons, *Adv. Appl. Probabil.*, Vol 27, 1995, p 384–396
91. A.M. Gokhale and A.K. Jena, Size Distribution of Grain Boundary Precipitates, *Metallography*, Vol 13, 1980, p 307–317
92. L.M. Cruz-Orive, Particle Size-Shape Distributions; the General Spheroid Problem, *J. Microsc.*, Vol 107, 1976, p 235–253
93. B.W. Silverman, M.C. Jones, D.W. Nychka, and J.D. Wilson, A Smoothed EM Approach to Indirect Estimation Problems, With Particular Reference to Stereology, *J. Royal Stat. Soc.*, Vol B52, 1990, p 271–324
94. S. Mase, Stereological Estimation of Particle Size Distributions, *Adv. Applied Probabil.*, Vol 27, 1995, p 350–366
95. A. Tewari, Ph.D. dissertation, Georgia Institute of Technology, 1999
96. K.S. Churn and R.M. German, *Metall. Trans. A*, Vol 15A, 1984, p 331–340
97. R.M. German, *Liquid Phase Sintering*, Plenum Press, 1985
98. H. Singh and A.M. Gokhale, Unpublished research, Georgia Institute of Technology, 2004
99. Z. Shan and A.M. Gokhale, Representative Volume Element for Non-Uniform Microstructure, *Comput. Mater. Sci.*, Vol 24, 20002, p 361–379